Lecture Notes in Electrical Engineering 133

Dehuai Yang
Editor

Informatics in Control, Automation and Robotics

Volume 2

Springer

Lecture Notes in Electrical Engineering

Volume 133

Dehuai Yang (Ed.)

Informatics in Control, Automation and Robotics

Volume 2

Springer

Dehuai Yang
Huazhong Normal Universiy,
Hubei,
China, People's Republic
E-mail: dehuai2020@126.com

ISBN 978-3-642-25991-3 e-ISBN 978-3-642-25992-0

DOI 10.1007/978-3-642-25992-0

Lecture Notes in Electrical Engineering ISSN 1876-1100

Library of Congress Control Number: 2011923552

Typeset by Scientific Publishing Services Pvt. Ltd., Chennai, India.

Printed on acid-free paper

9 8 7 6 5 4 3 2 1

springer.com

Foreword

2011 3rd International Asia Conference on Informatics in Control, Automation and Robotics (CAR 2011) is held on December 24–25, 2011, Shenzhen, China.

The purpose of the 2011 3rd International Asia Conference on Informatics in Control, Automation and Robotics (CAR 2011) is to bring together researchers, engineers and practitioners interested in the application of informatics to Control, Automation and Robotics.

The conference is organized in three simultaneous tracks:"Intelligent Control Systems and Optimization", "Robotics and Automation" and "Systems Modeling, Signal Processing and Control". We welcome papers from all these areas.

The book is based on the same structure, and topics of particular interest include, but not limited to: Intelligent Control Systems and Optimization, Robotics and Automation, Signal Processing, Systems Modeling and Control, Communication Theory and Technology, Sensor and sensor network, Computer Theory and Technology, Electrical and Electronic Engineering, Multimedia and Network Information, Photonic and Optoelectronic Circuits, Communication Systems and Information Technology, Electrical and Electronic Engineering, Signal Processing

Although CAR 2011 receives 850 paper submissions, only 219 where accepted as regular papers, based on the classifications provided by the Conference Committee and the reviewers. The selected papers also reflect the interdisciplinary nature of the conference. The diversity of topics is an important feature of this conference, enabling an overall perception of several important scientific and technological trends. These high quality standards will be maintained and reinforced at CAR 2011, and in future editions of this conference.

Furthermore, CAR 2011 includes 2 plenary keynote lectures given by internationally recognized researchers. They are Prof. Patrick S.P. Wang, Ph.D., Fellow, IAPR, ISIBM and WASE Northeastern University Boston, and Prof. Jun Wang, Department of Mechanical & Automation Engineering, The Chinese University of Hong Kong, Shatin, New Territories, Hong Kong. Their presentations presented an important contribution to increasing the overall quality of the conference, and are partially included in the first section of the book. We would like to express our appreciation to all the invited keynote speakers who took the time to contribute with a paper to this book.

On behalf of the conference organizing committee, we would like to thank all participants. First of all to the authors, whose quality work is the essence of the conference and to the members of the program committee, who help us with their expertise and time.

As we all know, producing a conference requires the effort of many individuals. We wish to thank all the people from IERI, whose work and commitment are invaluable.

Committee

Honorary Chair

ChinChen Chang	National Chung Hsing University,Taiwan
Patrick S.P. Wang	Fellow, IAPR, ISIBM and WASE Northeastern University Boston, USA

Program Co-chairs

Yuntao Wu	Wuhan University of Technology, China
Weitao Zheng	Wuhan University of Technology, China

Publication Co-chairs

Honghua Tan	Wuhan Insitute of Technology, China
Dehuai Yang	Huazhong Normal Universiy, China

International Committee

Wei Li	Asia Pacific Human-Computer Interaction Research Center, Hong Kong
Xiaoming Liu	Nankai University, China
Xiaoxiao Yu	Wuhan University, China
Chi Zhang	Nanchang University, China
Bo Zhang	Beijing University, China
Lei Zhang	Tianjin Institute of Urban Construction, China
Ping He	Liaoning Police Academy, China
Alireza Yazdizadeh	International Science and Engineering Center, Hong Kong
Wenjin Hu	Jiangxi Computer Study Institute, China
Qun Zeng	Nanchang University, China

Contents

Robotics and Automation

Simulation of Smog Diffusing Based on Particle Swarm Optimization

Jianfeng Xu[1], Lan Liu[3], and Qun Liu[2]

[1] College of Software, Nanchang University, Nanchang 330047
jianfeng_x@ncu.edu.cn
[2] Chongqing University of Posts and Telecommunications, Chongqing 400065
[3] Department of Computer Science & Application Technology,
Nanchang University, Nanchang 330031

Abstract. In the field of Computer Graphics the simulation of irregular fuzzy object still is a difficult challenge. Based on particle swarm optimization, the method of combining smog particle density diffusion and inter particles collision each other was studied in this research, which simulates the diffusing and real-time performance of smog. Diffuse force field was established by the diffusion equation, which could ensure the accuracy of the trajectories of diffusion. In order to reduce the time on collision between particles each other, a collision technology based on spatial hashtable is introduced in the research. Experimental results via simulation experiment show that the proposed method in the paper not only can improve the simulation speed of real-time requirements, but also demonstrate the authenticity of the smog diffusion.

Keywords: Particle swarm, Diffusion equation, Spatial hashtable, collision detection, Real time.

The simulation of irregular fuzzy object such as smog is one of the most difficult challenge in the field of Computer Graphics. It can't be accurately described in classic geometry, because of irregular shape and complicated transformation. However, with the development of the requirement increaseing of fuzzy object emulation in the filed of Moves, Games and Computer Cartoon,a lot of mew simulation methods come forth. The method based on particle swarm (a technology of simulate fuzzy object motion, which was proposed by Reeves [1] in1983) is used in many simulation of irregular fuzzy object . In the theory, object can be defined as particle set which is consist of thousands of irregular and random distribution particles. Every particle has individual attributions such as color, position, size and speed .And at every moment it consecutive moves and changes forms .In addition, it has a certain lifecycle which includes the process of birth, activity and death. So Particle Swarm can represent the modality of irregular fuzzy object just as motility, randomicity and the Visual authenticity.

The simulation of irregular fuzzy object based on Fluid function is another important method, which can display the authenticity of moving object by solving fluid equation.

Stam [2] combined semi Lagrangian method to implicitly resolved NS function, this method improved the development of the Fluid third dimension simulation. At the same time, Fedkiw [3]and Selle [4] are the outstanding representative of using

D. Yang (Ed.): Informatics in Control, Automation and Robotics, Volume 2, LNEE 133, pp. 1–8.
springerlink.com

hydrodynamics to simulate the movement of smog atoms. their job of simulant smog fuid has strong third dimension. Traditional method technology based on Particle Swarm Optimization can not solves the occasion of accuracy request [5,7]. Similarly, the method based on fluid function need calculate a great deal of function. Although, the method such as gridding and interpolation can improve the compute speed, the real-time reflection still is the bottleneck of the method using currently hardware. So it is important that combining the method of particle swarm and other physics models for the simulation of irregular fuzzy floating object.

After that, this paper imports a method based on space hash table [6], which is used to collision detection inside a deformable objects such as smog particles, to improve the efficiency of real-time reflection. While this simple and effective method be executed, the accuracy of collision simulation can be adjusted to accord the system's need and the time of collision detection can be greatly reduced.

Furthermore, the effect of density diffusion force is added to this paper to simulating the diffusion of smog accurately .The model ,which combined with the technology of particle swarm and other physics models, can balances the physical authenticity and the real-time ability of simulation . Finally this research gets better remarkable effect of simulation.

1 Density Diffusion

Suppose there is no effection of other factors such as earth and wing, the smog's diffusion in the endless space obeies the rule of heat exchange. Because the density of smog changes along with the diffusion, then the function of the density change can be expressed as Equation (1):

$$\begin{cases} \dfrac{\partial C}{\partial t} = k\left(\dfrac{\partial^2 C}{\partial x^2} + \dfrac{\partial^2 C}{\partial y^2} + \dfrac{\partial^2 C}{\partial z^2}\right), (-\infty < x, y, z < \infty, t > t_0) \\ C(x, y, z, t_0) = C_0(x, y, z) \end{cases} \tag{1}$$

In Equation (1): C as the density scalar quantity of density field, k as the diffusion coefficient, t0 as the time when the particle is created. Since function (1) just simulate the change of the density when the particle is created, C_0 should be zero as Equation(2).

$$C_0(x, y, z) = 0 \tag{2}$$

Then Equation (3) is the solution of equation (1) based on Equation (2), which was resolved by Jos Stam [5] and his partners.

$$C(x, y, z, t) = \frac{1}{(2k\sqrt{\pi(t - t_0)})^3} e^{-\frac{(x-x_0)^2 + (y-y_0)^2 + (z-z_0)^2}{4k^2(t-t_0)}} \tag{3}$$

In this Equation (3) (x_0, y_0, z_0) as the position of the smog source.

$$\text{If } \begin{cases} l = t - t_0 \\ r = \sqrt{(x - x_0)^2 + (y - y_0)^2 + (z - z_0)^2} \end{cases}$$

And l represents the currently particle alive time (life value currently), r as the distance from the particle to the source. So the equaption (3) can change to equation (4)

$$C(r, l) = \frac{1}{(2k\sqrt{\pi l})^3} e^{-\frac{r^2}{4k^2 l}} \tag{4}$$

It is a solution of equation (4), that the isosurface of density is a sphere which has equal radius, and the density continues degression with the enhance of the radius. As shown in Figure 1, the smog is diffusing from high density to low density.

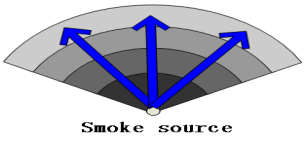

Fig. 1. Diffusion of smog

Suppose there is a smog particle in air, the distance from current position to the source is r_1, the current life-value is l_1, the distance from the position of prevframe to the source is r2, the life-value is l2, Next the density difference equation between the two frames should be Equation (5).

$$\Delta C = C(r_2, l_2) - C(r_1, l_1) \tag{5}$$

Based on ideal gas-state Function: $PV = nRT$, the pressure and the density are in the direct ratio, on the contrary the density difference will bring pressure and stress. For convenience, suppose the diffusing stress brought from density difference is Equation (6).

$$f_{diffusion} = \Delta C \times s \tag{6}$$

S is the constant which is proposed by experience value.

Since the smog diffuses along with the every direction of the sphere radius, the direction of $f_{diffusion}$ points from the source to the currently position. Though the power of density diffusion is more small than other powers, the effect to the track of smog movement is still important. So, if the power of the density diffusion be added, the stimulation of smog diffuse should be more true.

2 Inside Collision Detection

In the movement of smog particles, the collision between the particles can't be negatived. And the powers is the main reasons of smog diffusion which are produced from the collision. Obviously, the collisions between every two particles will spend great deal of times. Moreover the real-time requirement is difficulty to get, especially the number of the particles is large. So disposing collision detection and collision response is a very difficult question in computer graphics. Morever, it still is the focus

of computer graphics nowadays that how to abbreviate the time of collision detection and how to move of particles after collision .Thus, in the paper, Space Hash-Table and the Impulse theory are introduced to detect collision, and to accurately work out the particles moving states happened after the particles collision.

2.1 Space Hash-Table

Just like simple hash-table, space hash-table sets up a mapping relation between the data-entity and the data-address. using space hash-table, three-dimensional space can be divided into many little three-dimensional gridding. Moreover, the smog information of the system should be stored in the little three-dimensional gridding, and the index code of the three-dimensional gridding just as the smog particle memory address. For example, as shown in figure2, the two-dimensional space be divided into, 0、1、2、3, four little grid. the index codes of particles, A、B、C、D、E、F、G、H, which stay in the two-dimensional spaces are reflected by hash-table.

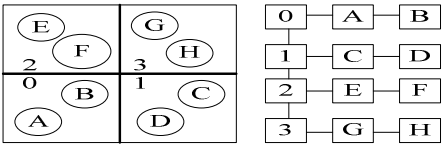

Fig. 2. Two-dimensional space and hash-table

2.2 Diffusion of Particle Space

In three-dimensional space, the hash-table key *d*ata h is the reflection of a three-dimensional particle(*x,y,z*): $h = hash(x, y, z)$. Then, this paper sets a special hash function according to the shape of smog. which can improve the average degree of diffusion. Since the direction of smog diffuses is from down to up, the *Y*-shaft has more long span than that of *X*-shaft or *Z*-shaft. Therefore, Y-shaft can be divided into several layers and each layer can be divided into four sections.

$$h(x, y, z) = D(y) \times 4 + D(x, z)$$

Thereinto,

$$D(y) = \begin{cases} 0 & y \le L \\ \lfloor y / L \rfloor & L < y < L \times (n-1) \\ n-1 & y \ge L \times (n-1) \end{cases}$$

$$D(x, z) = \begin{cases} 0 & x \ge 0, z \ge 0 \\ 1 & x < 0, z \ge 0 \\ 2 & x < 0, z < 0 \\ 3 & x \ge 0, z < 0 \end{cases}$$

In the Equation given above, L as the altitude of each layers, n as the number of layers. While this equation executing, particles can be equably distributed into hash-table and the hash collision can be reduced.

If the data structure of the above equation be defined, $C_i(0 <= i < n)$ should be the three-dimensional space whose key-data is i, S as the particles numbers in the space, and $p_{i,j}(0 <= j < m)$ as the first j particle in the first i gridding.

Similarly, every particles need some definite space, so particle border should be taked into account when particles distributing. Since particles can be regarded as a 3D square, the eight vertex of the 3D square should be reflected into hash-table which be considered as entire particle. So a particle maybe holds more than one three-dimensional gridding, and reflects more than one hash key data. Figure 3 is the example of the theory with two-dimensional space. Particle s holds four space of gridding such as 1、3、4、6, so the four gridding be reflected to hash-table as the entire particle S.

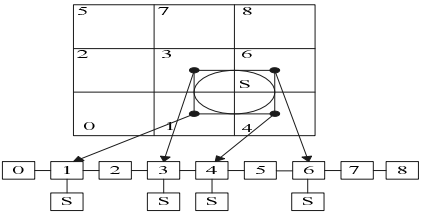

Fig. 3. A particle in several space gridding

2.3 Collision of Each Particles

In order to reduce the complexity of measuring the collision of each particles, this paper just detections this particles which in same gridding, namely, have same hash-table key.

If Particle p both in space C_i and C_j, the measuring to the collision of b should be separate into two sections include the collisions happens in C_i and it happens in C_j.So the pseudocode of colliding each Particle should be expressed as:

```
for (int i =0 to n-1)                    // Traversing from C0 to Cn-1
{ for (int j =0 to sizeof( Ci )-1 )      // Traversing each griddings
    for (int k =0 to sizeof( Ci )-1)     // Measuring each two Particles in one gridding.
{   if ( Pi,j != Pi,k )
        Collision detection ( Pi,j , Pi,k );     //Measuring
    }
}
```

As figure4 showing, particle S1 collide with particle S2, the movement speeds of the two particles S1 and S2 are v_{1-} and v_{2-} before collision, then the speeds change to v_{1+} and v_{2+} after collision. And parameter n is the unit vector of collision action line.

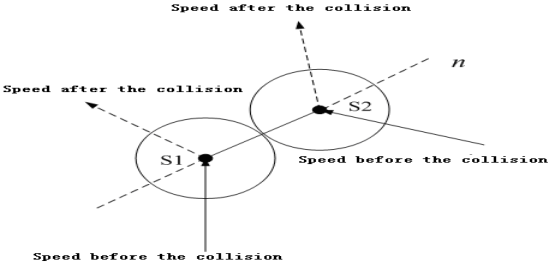

Fig. 4. Collision of two particles

For example there is a collision in one-dimensional space, the speeds of particles after collision can be resolved by momentum conservation theorem. According to condition, there are three equations:

$$J = m_1(v_{1+} - v_{1-}) \tag{7}$$

$$-J = m_2(v_{2+} - v_{2-}) \tag{8}$$

$$e = -(v_{1+} - v_{2+})/(v_{1-} - v_{2-}) \tag{9}$$

Equation (7) and (8) are impulse theorem, Equation (9) is function of resuming parameter. In above equation, m1 and m2 separately express the quality of S1 and S2, J as the impulse data by collision, e is the resuming parameter of collision which is a constant depended on material and structure of object, while the impulse direction of S1 is contrary for S2. Equation (7) and (8) can be changed to Equation (10) and (11).

$$v_{1+} = J/m_1 + v_{1-} \tag{10}$$

$$v_{2+} = -J/m_2 + v_{2-} \tag{11}$$

Then, v_{1+} and v_{2+} be substituted to Equation (9). Equation (12) should be educed.

$$J = -(v_{1-} - v_{2-})(e+1)/(1/m_1 + 1/m_2) \tag{12}$$

And the speeds of two particles after collision should be resolved when equation (12) be substituted to equation (10) and (11). But, in three-dimensional space, speed should be changed to vector, only the speed changing should produce impulse of which the direction is the same as the normal line, and only the component of the impulse can influence the speed. So the equation (12) can be changed to equation (13).

$$J = \frac{-(v_{1-} - v_{2-})(e+1)\bullet n}{1/m_1 + 1/m_2} \tag{13}$$

And equation (10) and (11) can educe the equation as follows.

$$\begin{cases} v_{1+} = J\bullet n/m_1 + v_{1-} \\ v_{2+} = -J\bullet n/m_2 + v_{2-} \end{cases}$$

Finally, when above equation be substituted equation (13), the speeds after collision, v_{1+}, and v_{2+}, can be educed.

$$v_{1+} = v_{1-} - \frac{(v_{1-} - v_{2-})(e+1)}{1 + m_1 / m_2}$$

$$v_{2+} = v_{2-} + \frac{(v_{1-} - v_{2-})(e+1)}{1 + m_2 / m_1}$$

In addition, after collision, the two particles consecutive movement with the speeds of v_{1+}, and v_{2+}, then the two particles collide with other particles in the same one frame , and the collision should be detectiond sequentially .

3 Simulation Experiment

In the phase of simulation, smog particles be Rendered based on particles swarm optimization method union texture mapping and billboard technologys. In this way, a texture piece can instead of many particles, so computing resource be saved and the rendering speed be improved. In this paper, the texture with size of 40×40 be used to particle map, and simulating big particles be adopted.

This algorithm had been realized by use Personal computer. Hardware environment include CPU：INTEL E2180, graphics card: Gforce 7300GT 128M, EMS memory：1GB RAM. R&d platform is VS2005 C++. Figure 5 is the diffusing phenomena of smog which be affected by random wind. Figure 6 is the exhaling phenomena of smog, which be produced by the collision of smog and sphere in space.

Fig. 5. Smog freely diffuse in the wind

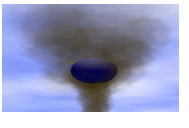

Fig. 6. Smog diffuse while the particles collide in space

Table 1. The comparison results of the algorithms

Emission rate of particle（A/SEC）	Frames per second of this algorithm	Frames per second of this traditional Particle System algorithm
10	72	46
20	60	32
30	51	22
40	43	17
50	38	14

Finally, this algorithm be compared with particle system method which be proposed in reference [1]. In the experiment, 32 grids be adopted in hash-table, the height of 3D grid is $L = 100$, the number of layers is n =8, the recovery coefficient of collision is $e = 0.5$ .The proportional constant of consistenceis diffusive force is $s = 0.1$. The life cycle of particle between 6 sec to 8 sec. The comparison results be showed in Table 1.

As Table1 shown, the algorithm of this paper is faster than traditional particle system algorithm .Similarly the more numbers of particles in the system, frame rate more than 20, the less real-time could be achievedwhile traditional particle system algorithm be used, however the algorithm of this paper can get better performance.

4 Conclusion

This study of simulating the smog particle diffusion is based on the particle swarm technology, Kinetics and the method of collision detection based on space hash-table. And the effect of density diffusion force is added to the scene.

The result of the above method has better performance such as Real-time, physical authenticity and visual authenticity than traditional method. The main research of the next step includes two main aspects. firstly, there is a interesting study of polymerization and deformation effect after the collision of particles . Secondly, the photosensitive photos of smog particles should be simulated, so that the emulation effect may be improved. Above research can be widely used to environment detection, air pollution index measure, etc.

References

1. Reeves, W.T.: Particle Systems–A Technique for Modeling a Class of Fuzzy Objects. Computer Graphics 17(3), 359–376 (1983)
2. Stam, J.: Stable fluids. In: Proceedings of SIGGRAPH, Los Angeles, California, USA, pp. 121–128 (1999)
3. Fedkiw, R., Stam, J., Jensen, H.: Visual simulation of smoke. In: Proceedings of SIGGRAPH, Los Angeles, California, USA, pp. 15–22 (2001)
4. Selle, A., Mohr, A., Chenney, S.: Cartoon rendering of smoke animations. In: Proceedings of the 3rd International Symposium on Non-Photorealistic Animation and Rendering, Annecy, France, pp. 57–60 (2004)
5. Zhuo, N.-W., Rao, Y.-B.: Real Time Dense Smoke Simulation Based Particle System. In: IITAW 2008, pp. 809–813 (2008)
6. Teschner, M., Heidelberger, B., Muller, M., Pomeranets, D., Gross, M.: Optimized spatial hashing for collision detection of deformable objects. In: Proceedings of Vision, Modeling, Visualization, VMV 2003, pp. 47–54 (2003)
7. Zhang, Q., Xie, J., Wu, H.: Of such of Research review of Modeling method for irregular objects: Fire, smoke and clouds China. Image and Graphics Academic Journal 5(3), 186–190 (2000)
8. Zhan, Y., She, M., et al.: Real time cartoon smog simitation algorithm based on physics model, China. Image and Graphics Academic Journal 12(2), 261–265 (2007)

Self-compensating Technology for Disturbing Torque of Space Swing Camera

Wang Xiaoyong

Northwestern Polytechnical University, Xi'an, 710072
w8320@126.com

Abstract. The disturbing torque generated by space swing camera during imaging affects the attitude stabilization of satellite. To solve this problem, self-compensation technology for reducing disturbing torque of camera was proposed. By using self-compensating equipment and synchronization control technology, 90% of the disturbing torque generated by camera can be reduced, hence the significant reduction in its influence on the satellite stability. Through simulation and testing, the technology was proved to be able to reduce the disturbing torque by camera significantly and meets the requirement of satellite attitude control.

Keywords: swing camera, disturbing torque, self-compensation, satellite attitude.

1 Introduction

Satellite-carried swing camera uses lateral scanning and imaging technology to fulfill the extra-wide land coverage. The optical system of the camera adopts the all reflecting optical system with little angle of field and small relative aperture, with built-in scanning reflection lens in front of the camera's optical system. The camera provides enlarged scanning coverage through lateral scanning along the path vertical to the satellite flight direction. In order to compensate the velocity of image motion produced by the satellite forward movement during imaging process, the camera's optical axis needs to process image compensation along the opposite direction of the satellite flight trajectory, as illustrated in Fig. 1:

When a satellite flies along its trajectory, a complete action cycle is indicated from point A to point D. From A to C, the camera scanning reflection lens rotates with constant speed along x-axis (satellite flight direction) to scan from left to right during imaging process; From B to C, the camera produces image of the right area; From C to D, the camera reflection lens rotate in opposite direction along x-axis until the scanning reflection lens backs to the original position, which concludes a complete working cycle.

A satellite uses three axis stable attitude control mechanism. Its attitude stability requires to be 0.005˚/s (3σ). Due to the disturbing torque generated during the scanning process by scanning reflection lens that hampers the attitude stability as well as image quality, it is necessary to compensate the disturbing torque generated in scanning reflection lens movement.

D. Yang (Ed.): Informatics in Control, Automation and Robotics, Volume 2, LNEE 133, pp. 9–17.
springerlink.com

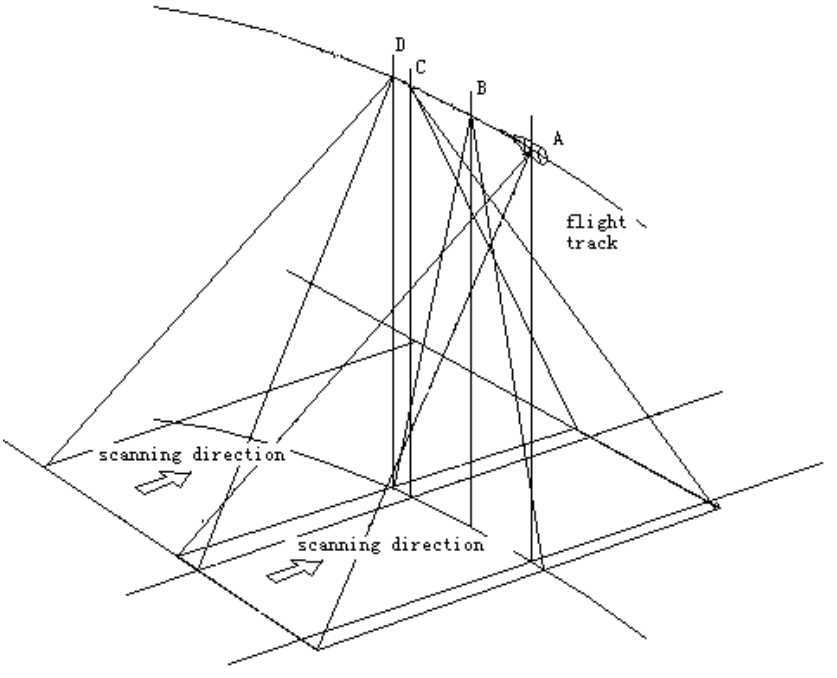

Fig. 1. Scan imaging mechanism illustration

2 The Disturbing Torque Self-compensation Proposal

The printing area is 122 mm × 193 mm. The text should be justified to occupy the full line width, so that the right margin is not ragged, with words hyphenated as appropriate. Please fill pages so that the length of the text is no less than 180 mm, if possible.

Swing camera is tilt positioned on the satellite to fulfill image compensation. The scanning axis of the scanning reflection lens was positioned at the angel of α=3.6340 in plane X_bOY_b, inertia of the scanning lens along the rotation axis J=0.035kgm2, the damped coefficient is 0.0188kgm2/s. The camera scans along with single axis cyclically, with cycle time of 6.28s. The scanning movement equation is as below:

$$\omega_x = 10.396t \qquad 0 \leqslant t \leqslant 0.205s \tag{1}$$

$$\omega_x = 2.151 \qquad 0.205s \leqslant t \leqslant 4.205s \tag{2}$$

$$\omega_x = 2.151 - 10.296(t - 4.205) \qquad 4.205s \leqslant t \leqslant 5.345s \tag{3}$$

$$\omega_x = -9.693 + 6.997(t - 5.345) \qquad 5.345s \leqslant t \leqslant 6.28s \tag{4}$$

The disturbing torque generated by camera scanning lens movement is illustrated by Fig.2:

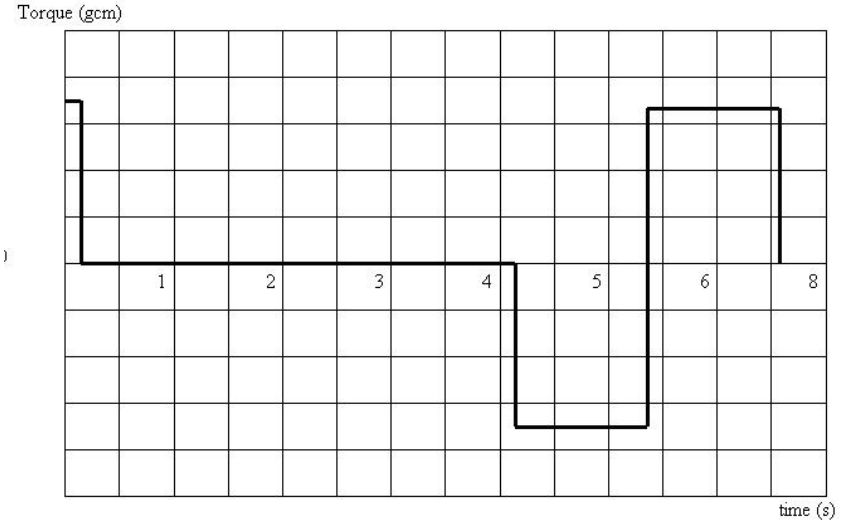

Fig. 2. Camera scanning disturb torque curve

With the anti-disturbing torque equipment installed on the camera, when scanning lens are moving, the anti-disturbing torque equipment generates the disturbing torque opposite to the scanning lens movement direction. By doing so the self-compensation is achieved.

Camera disturbing torque self-compensation mechanism uses electrical synchronous mechanical torque compensation technology through the shafting of the torque compensation momentum wheel installed on the camera. The rotation inertia of scanning mirror equals to that of momentum wheel carried on torque self-compensation equipment. The torque compensation equipment leverages the same kind of motor that has the similar torque feature curve observed in the scanning driving motor, is driven by the same source of power, and has the same damping torque. The control power drives the opposite direction movement of scanning mirror and momentum wheel. When the motor driven camera scanning mirror makes the swing movement of±4.5°, the momentum wheel of the torque compensation system does the same pendular movement of±4.5° in the opposite direction, hence the torque compensation is achieved via torque balancing, resulting in the elimination of most of disturbance generated by the pendular movement of camera, and rendering less than 10% compensation accuracy variation.

In simulation of total output torque of the camera with torque compensation, assume compensation accuracy variation is less than 10% and response time no greater than 10ms, the output disturbing torque after compensation is charted in Fig. 3.

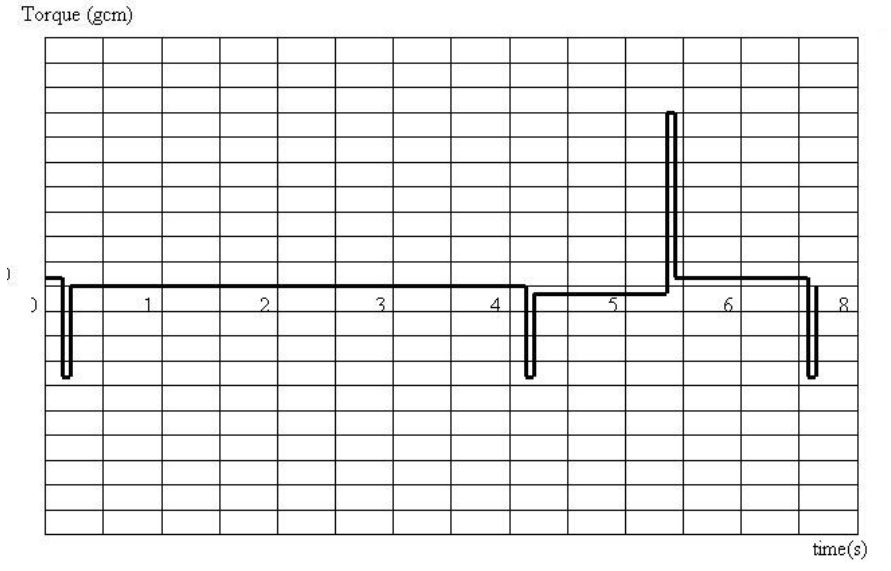

Fig. 3. Residual Torque Curve After Camera Compensation

3 Satellite Attitude Mathematical Simulation Analysis

The following two steps are used to analyze the mathematical simulation of the satellite attitude with the existence of disturbing torque:
Firstly, without the consideration of disturbing torque, analyze the impact on satellite attitude based on the established model parameters of camera scanning equipment.

Secondly, with the consideration of disturbing torque, analyze the impact on satellite attitude based on the established model parameters of camera scanning equipment and torque compensation equipment.

Based on the general satellite feature, assume the following satellite quality parameters:

Weight M=600kg, rotation inertia Ixx=193 kgm2, Iyy=70 kgm2, Izz=204 kgm2 Based on the camera structure feature, assume the camera scanning reflection lens are ellipse, long axis =220mm, short axix=140mm, weight=0.98kg, rotation inertia=0.04 kgm2.

3.1 Simulation Analysis without Self-compensation

Based on the simulation of the scanning movement according to the given ideal movement equation without camera torque self-compensation, satellite attitude

stability during camera imaging process is charted in Fig. 4. It is shown that rotation angel speed has been impacted significantly. rotation angel speed on steady state was larger than 2×10-3o/s. The fluctuation was obviously observable.

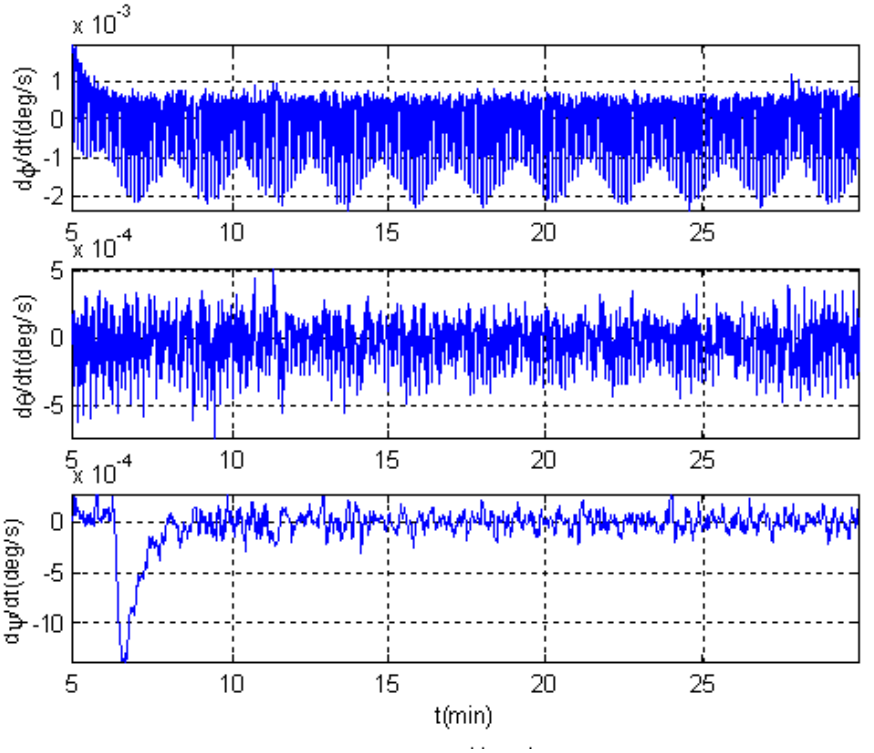

Fig. 4. Satellite Attitude Angel Speed Simulation Curve (without scanning torque self-compensation)

3.2 Simulation Analysis with Self-compensation

With torque self-compensation, due to the synchronization phase difference existent in scanning and compensation, the torque on x-axis of the satellite in a short period of time was 0.0086×2=0.0172Nm. In the simulation, the phase difference of camera pendular movement and compensation driving movement was set up as 10ms. Fig. 5 shows the satellite attitude simulation curve. Compared with the result without self-compensation, the satellite attitude angel speed has improved significantly. The rotation angel speed on steady state was less than 5×10-4o/s.

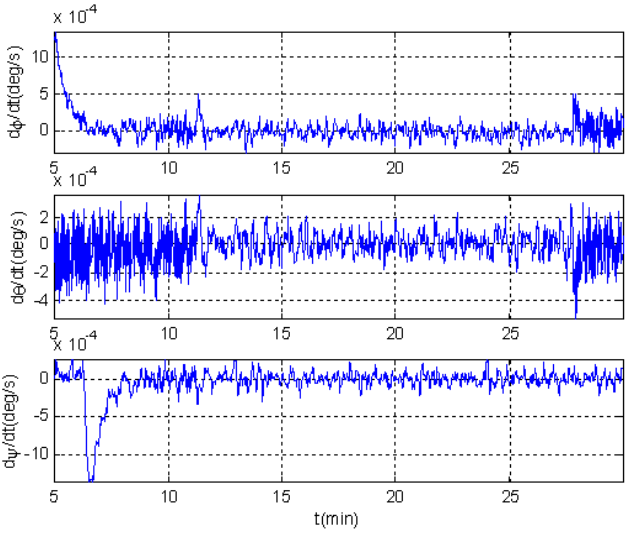

Fig. 5. Satellite Attitude Angel Speed Simulation Curve (with scanning torque compensation)

4 Disturbing Torque and Self-compensation Effect Test

To prove the effectiveness of anti-torque compensation equipment technology, camera torque compensation test was conducted. To precisely capture the impact of scanning movement on satellite attitude, the scanning torque disturbance was measured on a single-axis flotation physical simulation platform. The measurement was charted in the Fig.6. The chart shows that the disturbing torque generated in the camera movement without self-compensation equipment installed is no greater than 8.5 gcm.

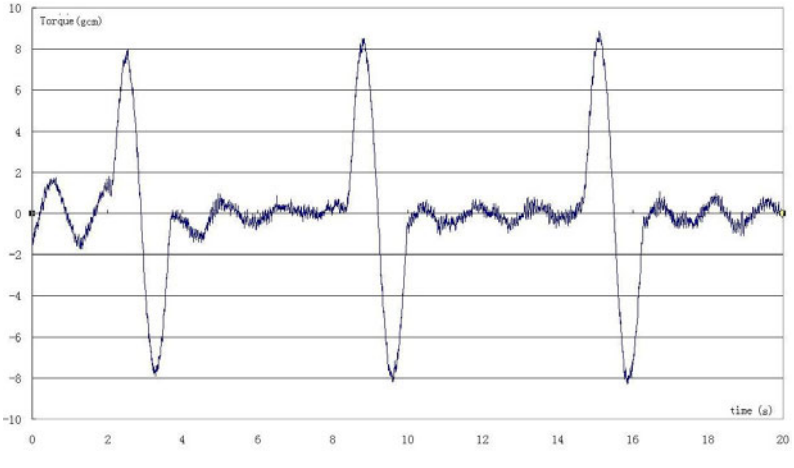

Fig. 6. Camera Disturbing Torque Measurement (without self-compensation)

Further measurement on disturbing torque was conducted when self-compensation was adopted. The measurement result is shown in Fig.7. The chart shows that the disturbing torque generated in the camera movement with self-compensation equipment installed is no greater than 2 gcm.

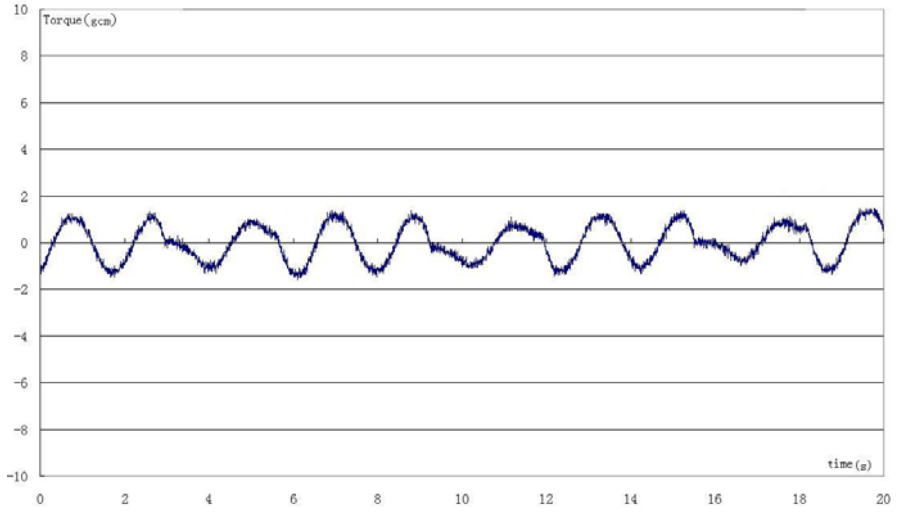

Fig. 7. Camera Disturbing Torque Measurement (with self-compensation)

After the camera scanning torque disturbance test was completed and the relevant data was captured, a mechanics coupling physical simulation test of swing camera and satellite control system was implemented. The test system is composed of wide-coverage camera system, satellite attitude control system, momentum wheel, satellite rotation inertia analogy module, etc.

During the test, after the camera's scanning movement, the attitude control systems controls the satellite according to the given parameters. Fig.8 shows the test result. In the diagram, horizontal axis means time, the three graphs on the right hand side show 1) offset of satellite attitude angel, 2) offset of satellite attitude angel speed, and 3) offset of rotation speed of the satellite control system execution element -- momentum wheel, respectively.

It is observed from the measurement curve that with camera self-compensation, under the impact of disturbing torque generated in camera imaging process, the satellite attitude angel accuracy variation is less than 0.01 °; the attitude angel speed control accuracy variation is less than 0.001 °/s, which has met the requirements that 1) satellite control attitude stability should be no greater than 0.005°/s, 2) has no impact on imaging process, and 3) momentum wheel is within the saturation control range.

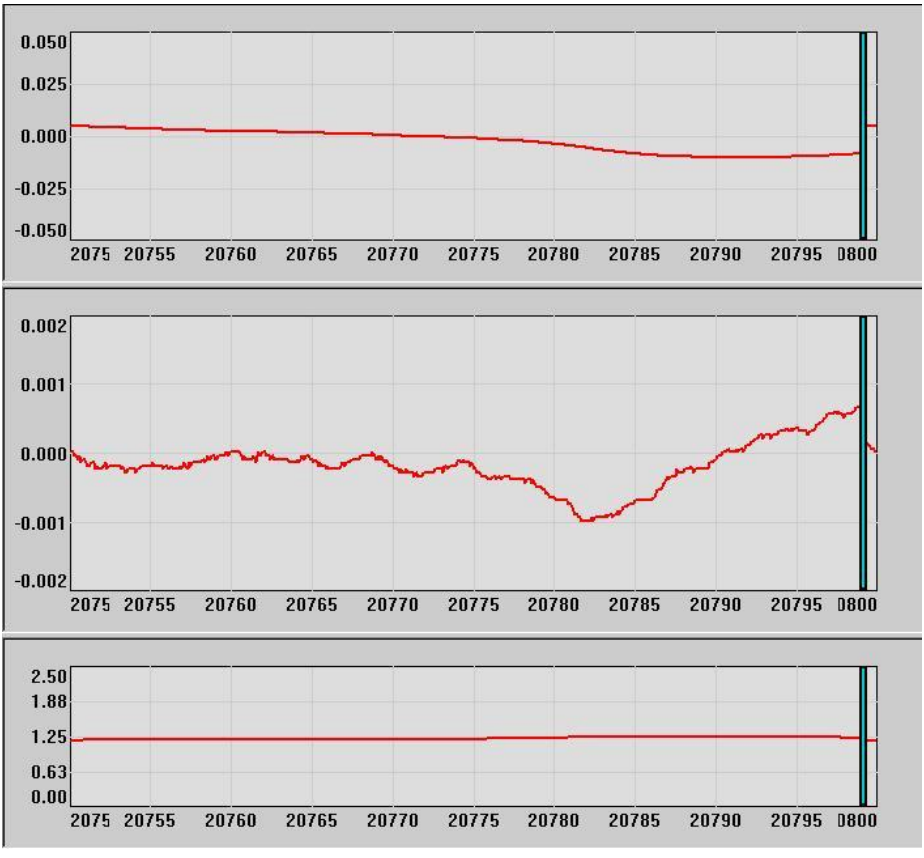

Fig. 8. Mechanics Coupling Physical Simulation of Camera and Satellite Control System Test Result

5 Conclusion

Satellite carried space swing camera influences the satellite flight attitude during the imaging process, which in turn influences the image quality. In response to this problem, a self-compensation solution by installing anti-torque compensation equipment on the camera was proposed. To prove the effectiveness of the torque compensation, mathematical simulation and physical simulation testing were implemented to measure the fluctuation generated by camera scanning movement before and after the compensation equipment was installed. The test result shows the compensation effectiveness of greater than 90%, and the residual torque disturbance reduction to less than 10% of its original level. The technology has met the stability requirement. With proven feasibility, it can be applied to all kinds of satellite space swing cameras.

References

1. Liu, W., Yao, D.-Z., Hua, Y.-Y., Wu, J.-W.: The Design of TDI CCD Camera System. Infrared Technology 32(9), 505–508 (2010)
2. Fan, C., Li, Y.-C., Yi, H.-W.: Influence Analysis of Buffeting on Image quality of TDICCD Camera. Acta Photonica Sinica 36(9), 1714–1717 (2007)
3. Fan, C., Li, Y.-C., Yi, H.-W.: Influence analysis of drift angle on image quality of TDICCD camera. Opto-Electronic Engineering 34(9), 70–73 (2007)
4. Zhang, Y.-X., Liu, Y., Ge, W.-Q.: Development and prospect of image motion compensation technology. Chinese Journal of Optics and Applied Optics 3(2), 112–118 (2010)
5. Liu, M., Wu, H.-S., Kuang, K.-P., Xiu, J.-H.: Image motion compensation in aerospace camera. Optics and Precision Engineering 12(z2), 30–32 (2004)

Matrix Multiplication Parallelization on a Many-Core Platform

Pollawat Thanarungroj and Chen Liu

Department of Electrical and Computer Engineering
Florida International University Miami, Florida, USA
{pthan001,cliu}@fiu.edu

Abstract. This paper introduces an approach to analyze the power and energy consumption of a many-core system. The investigation has been done by using the Intel SCC system as an experimental platform. The approach is to collect the time and power profiling of an executing application on the Intel SCC system. And then, we find the total energy consumed for the entire execution. We studied the effects of power and energy consumption in many-core systems by varying different hardware configuration parameters such as number of cores, clock frequency and voltage level. Thus, the many-core system can be explored for its scalability, fitness in operational cost and performance.

1 Introduction

Many hardware techniques have been proposed to increase the parallelization of these transistors. Lots of hardware implementations are already existed for parallelizing sequential program execution such as Superscalar, Superpipelining, Simultaneous Multithreading (SMT)[1-2], Chip Multiprocessors (CMP) [3] (also known as multi-core processors) and most recently, many-core processors.

There are advantages that multi-core and many-core gain while single core processor does not [3-5, 16-18]. Both multi-core and many-core processors gain the benefit from shorter wiring which minimized the delay among cores instead of going off-chip. Similarly, in multi-core and many-core processors power and energy consumption increase linearly when the number of cores increases; while increasing the complexity in single processor design, it consumes a quadratic increase or even more in power and energy consumption. Moreover, the use of identical processing elements in homogeneous architecture reduces the complexity of hardware design and verification hence the entire development cycle.

The Single Chip Cloud Computer (SCC) experimental processor [6-10] is a 48 core 'concept vehicle' created by Intel Labs as a platform for many-core software research. This SCC system is a second generation processor design that has been successfully developed by Tera-Scale Computing Research Program. SCC is the microprocessor system that has the highest number of cores integrated onto a single chip which intended to encourage more researches on many-core processor research and parallel programming research. The many-core processor researches [11] are high-performance power-efficient fabric, fine-grain power management and message-based programming support.

D. Yang (Ed.): Informatics in Control, Automation and Robotics, Volume 2, LNEE 133, pp. 19–26.
springerlink.com

SCC is a research platform that allows voltage and frequency scaling. Thus, it is possible to derive the power and energy consumption characteristics of the SCC by applying different frequency and voltage configuration to the different cores. We observe the power and energy scalability of the SCC system by executing a program with different numbers of cores. By performing such experiment, we can also verify that the message passing interface can hold the power and energy consumption scalability.

The rest of the paper is organized as follows. In Section 2 we discuss on our matrix multiplication test program. In the later section, we present our results from varying the number of cores and varying two different frequency and voltage level of all the cores. Finally, a conclusion is presented in Section 4.

2 Experimental Setup

In our experiment, we implemented our work on SCC system with SCCKit version 1.4.0. SCC system setup consists of two components, one is SCC itself and the other one is called Management Console Personal Computer (MCPC). MCPC is installed with a 64-bit Linux operating system, Ubuntu 10.04 in this case. MCPC system supports basic C programming language compilers such as gcc, g++, icc and icpc. Moreover, MCPC also supports the need of FORTRAN compiler ifort and MKL compilers mkl. The executables are generated by MCPC and run on the SCC cores.

We implemented a mixed sequential and parallel workload program that performs a multiplication of two matrices (C=A*B). We tried to imitate the program behavior according to the original program in [12, 13]. This program is written based on C programming language. To calculate the value of C=A*B in parallel the program executes as follows. First, we assign one of the cores as root core and other cores as computing core. At the beginning of the program, the root core creates matrix A and matrix B. The value of the elements in matrix A are calculated by summing up the x-y coordinates of the matrix. The value of the elements in matrix B are calculated by multiplying the x-y coordinates of the matrix. Then, the root core divides matrix A into different number of rows and distributes the fragments of matrix A to other executing cores. Root core also sends the information of the offset of the fragmented matrix A, number of rows of matrix A and the entire matrix B to be multiplied with. This centralized communication within the root core is the sequential part of the program execution. To plot the experimental data, the longer program execution yields a clearer graphical plot. Therefore, in this experiment, we assigned 3,000 rows in matrix A and 150 columns in both matrix A and matrix B. The matrix multiplication program has been implemented on icc compiler version 8.1.038 with the optimization flag O3. Only the matrix multiplication calculation itself can be computed in parallel but there are overheads that cannot be parallelized such as the overheads from data communication, conditional loop, timer, measurement and results collection. An execution flow of our matrix multiplication program is illustrated in Fig. 1.

RCCE [14-15] is a specific API library for programming the message passing functions in SCC system. RCCE library has been inserted into the matrix multiplication program to adjust the frequency and voltage level on the SCC cores. There are two sets of setups in our experiment. First, we set the frequency and voltage of every core to 800 MHz and 1V respectively. Second, we set the frequency and voltage of every core to 400 MHz and 0.7V respectively. These settings apply to all the computing cores and also the root core. By varying the number of cores, we are able to observe time, power and energy characteristics. Because not all cores are involved in the computation, there will be idle cores which are needed to be taken into consideration. Due to the fact that we cannot completely turn off any core even it is in an idle state, we put the idle cores into the lowest stable operational frequency of 200 MHz with a supplying voltage of 0.6V. The operating frequency was fixed at the beginning of the execution. Thus, the program was executed at the same frequency and voltage until the program finishes its execution.

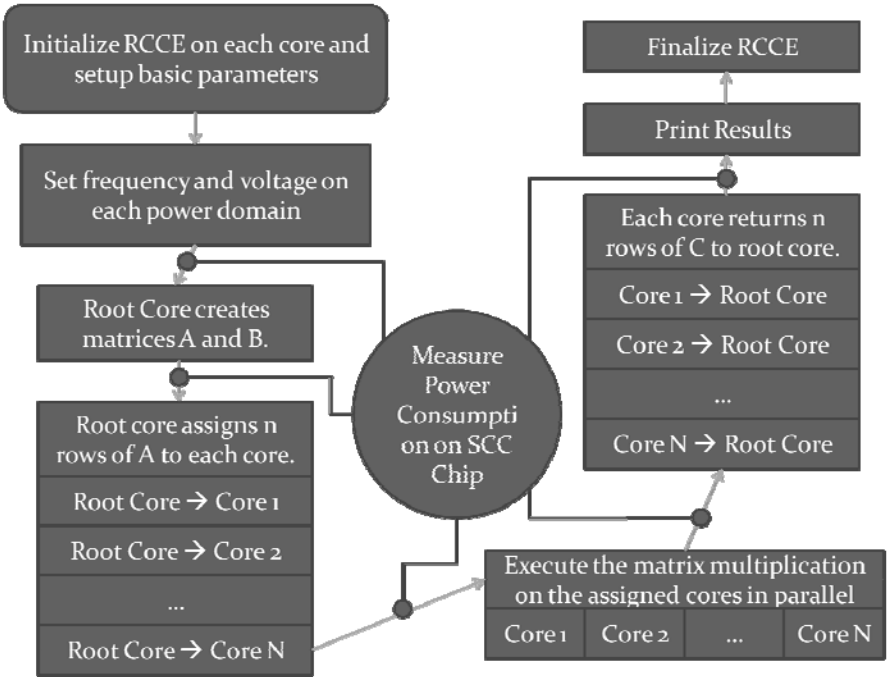

Fig. 1. Matrix multiplication program execution flow

In order to observe the power and energy consumption characteristics, we implemented a software design that can fetch the reading of the instantaneous power consumption of the SCC chip. The code was merged into the matrix multiplication program. To counter the time spent to stop the execution of the matrix multiplication program in order to get the power reading, we modified the matrix multiplication program so that it is now containing a RCCE timer which only counts when the program is running and stops counting when the program is fetching the

instantaneous power measurement from the SCC chip. However, to start and stop timer is not enough to totally eliminate the overheads from such context switching. Other timing overheads include frequency switching at the beginning of the execution and power measurement all along the execution which cannot be easily removed. We try to run our program long enough so that those overhead has the least effect on our results. As we execute the matrix multiplication program, we performed the power measurement 5 times in total. The power measurement cannot be done during the multiplication on each core is being computed because the power measurement will interrupt the sequential communication between root core and executing cores. An executing core returns its own computed result only when the result is completed. Hence, the completeness sequence from each core cannot be predicted. The power measurement is needed to be done after the all the executing cores have finished their computation to avoid the interruption. The power measurement involves the product of the total voltage dropped on the SCC chip and the total current flowed through the SCC chip. The measurement is similar to the one done by the GUI performance meter provided by SCC. At the end of the matrix multiplication program, the overall average power consumption was calculated from the mean of all power measurements done within the execution. We execute the matrix multiplication program starting from two cores all the way to entire 48 cores.

3 Experimental Results

The experimental results are separated into two sets, the setup with frequency of 800MHz and the setup with frequency of 400MHz. In our experiment, we recorded total execution time and average power consumption of the entire execution. Then we calculate total energy consumed by the SCC chip during the execution by multiplying the recorded total execution time and the recorded average power consumption. Therefore, we have three different parameters for each execution on the SCC system: total elapsed time, average power consumption and total energy consumption.

Firstly, Fig. 2 presents the relationship between the number of cores utilized for the matrix multiplication execution and the time it takes to finish the execution. We can obviously see that the total execution time needed to finish the matrix multiplication program in 800MHz frequency case is much less than the frequency of 400MHz. Despite the results showed that we can reduce the execution time by increasing the number of cores within the 48 cores execution, the time decays does not convince us to massively increase the number of cores because it is an exponential decay that slowly converges to a time instant. This limitation cannot be resolved due to the on-chip communication overhead among the cores. The total execution time gap between the 800MHz and 400 MHz frequencies are close to each other as the number of cores increases.

Secondly, Fig. 3 presents the relationship between the number of cores utilized for the matrix multiplication execution and the average power consumption of the entire execution. There is a dramatic increase in power consumption for the 800MHz frequency setup. The power consumption increases almost linearly when the number of cores increases for both operational frequencies. The average power consumption slope of the 800MHz frequency execution is much higher than the one from 400MHz frequency execution. Hence, the number of cores has less contribution to the power consumption for low frequency execution.

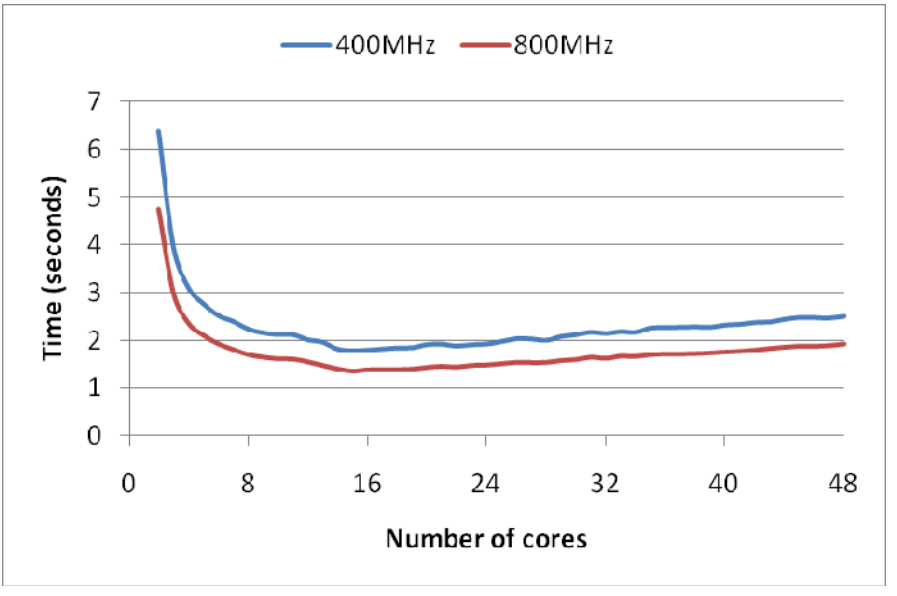

Fig. 2. Execution time comparison between 400MHz and 800MHz

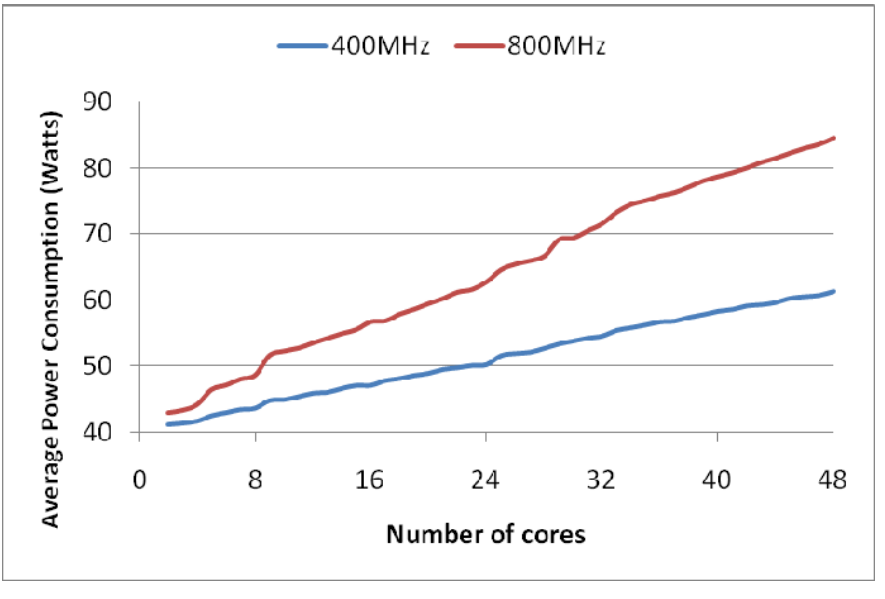

Fig. 3. Average power consumption comparison between 400MHz and 800MHz

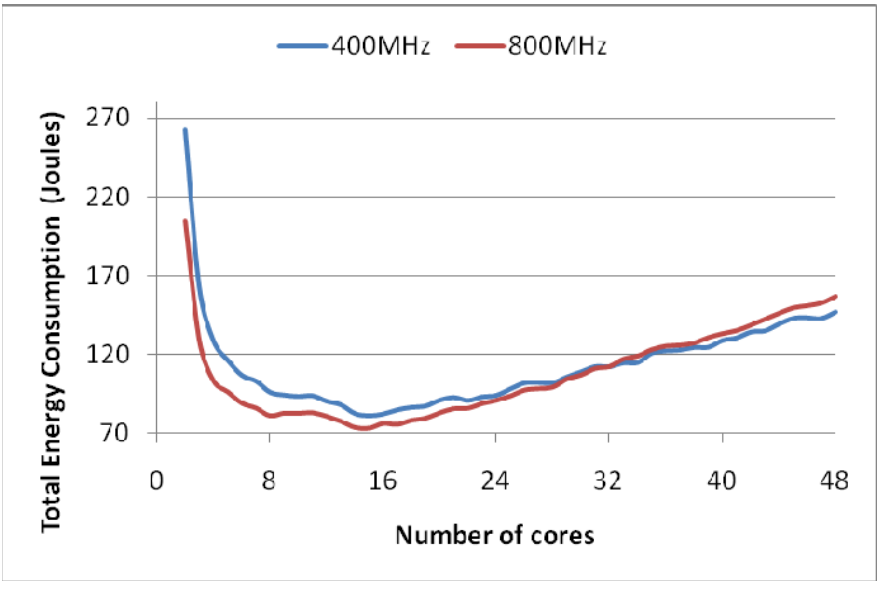

Fig. 4. Overall energy consumption comparison between 400MHz and 800MHz

Lastly, Fig. 4 presents the relationship between the number of cores utilized for the matrix multiplication execution and overall energy consumption of the entire execution. This plot represents the multiplication product of Fig. 2 and Fig. 3. On the left of the intersection with the number of cores lowers than 34, the frequency operation of 800 MHz needs less energy consumption than the 400MHz frequency. At 34 cores the total energy consumption of 400MHz is first less that the total energy consumption of 800MHz. Therefore, in term of energy optimization, we better run the program at high frequency for lower number of cores and run the program at low frequency for higher number of cores. Moreover, the results from 800MHz frequency shows that after 34 cores if we keep increasing the number of cores, instead of saving the energy, it will consume more energy to keep all the cores busy. The lowest energy consumption of 800MHz frequency operation is at 34 cores which mean we should not increase the number of core more than 34 cores on this configuration. Otherwise, it will consume more energy in order to execute the same amount of workload.

4 Conclusion

In this paper, we have investigated the time, power and energy relationship in a many-core system, SCC. Our results show that there is a boundary on the number of cores in many-core system and we realized that power consumption of a many-core system has an almost linear characteristic increment with the number of cores for a mixed sequential and parallel program execution. Our experimental results suggest us to run higher number of cores at low frequency operation and run lower number of cores at high frequency operation to optimize energy consumption of SCC system.

Acknowledgment. We would like to thank Intel Labs for providing us with SCC system in material transfer to conduct this research. This work is partly supported by the National Science Foundation under grant number ECCS-1125762. Any opinions, findings, and conclusions or recommendations expressed in this material are those of the authors and do not necessarily reflect the views of the National Science Foundation.

References

1. Tullsen, D.M., Eggers, S.J., Levy, H.M.: Simultaneous multithreading: Maximizing on-chip parallelism. In: Proceedings of 22nd Annual International Symposium on Computer Architecture, June 22-24, pp. 392–403 (1995)
2. Eggers, S.J., Emer, J.S., Leby, H.M., Lo, J.L., Stamm, R.L., Tullsen, D.M.: Simultaneous multithreading: a platform for next-generation processors. IEEE Micro. 17(5), 12–19 (1997)
3. Lance, H., Basem, N.A., Kunle, O.: A Single-Chip Multiprocessor. IEEE Computer 30(9), 79–85 (1997)
4. Flynn, M.J., Hung, P., Rudd, K.W.: Deep submicron microprocessor design issues. IEEE Micro. 19(4), 11–22 (1999)
5. Flynn, M.J., Hung, P.: Microprocessor design issues: thoughts on the road ahead. IEEE Micro. 25(3), 16–31 (2005)
6. Mattson, T.G., Van der Wijngaart, R.F., Riepen, M., Lehnig, T., Brett, P., Haas, W., Kennedy, P., Howard, J., Vangal, S., Borkar, N., Ruhl, G., Dighe, S.: The 48-core SCC Processor: the Programmer's View. In: 2010 International Conference for High Performance Computing, Networking, Storage and Analysis (SC), pp. 1–11, 13–19 (November 2010)
7. Howard, J., Dighe, S., Hoskote, Y., Vangal, S., Finan, D., Ruhl, G., Jenkins, D., Wilson, H., Borkar, N., Schrom, G., Pailet, F., Jain, S., Jacob, T., Yada, S., Marella, S., Salihundam, P., Erraguntla, V., Konow, M., Riepen, M., Droege, G., Lindemann, J., Gries, M., Apel, T., Henriss, K., Lund-Larsen, T., Steibl, S., Borkar, S., De, V., Van Der Wijngaart, R., Mattson, T.: A 48-Core IA-32 message-passing processor with DVFS in 45nm CMOS. In: 2010 IEEE International Solid-State Circuits Conference Digest of Technical Papers (ISSCC), pp. 108–109, 7–11 (February 2010)
8. Intel Labs, SCC Platform Overview. Intel Many-core Applications Research Community, Revision 0.75 (September 2010)
9. Jim, H.: Single-Chip Cloud Computer. In: Intel Labs Single-chip Cloud Computer Symposium (February 2010)
10. Salihundam, P., et al.: A 2 Tb/s 6 4 Mesh Network for a Single-Chip Cloud Computer With DVFS in 45 nm CMOS. IEEE Journal of Solid-State Circuits 46(4), 757 (2011)
11. Intel-Tera Scale Computing Research, `http://techresearch.intel.com/ResearchAreaDetails.aspx?Id=27`
12. National Center for Computational Science, `http://www.nccs.gov/user-support/training-education/hpcparallel-computing-links/mpi-examples/`
13. Snir, M., Otto, S., Huss-Lederman, S., Walker, D., Dongarra, J.: MPI: The Complete Reference. MIT Press (1996)

14. Van der Wijngaart, R.F., Mattson, T.G., Haas, W.: Light-weight communications on Intel's single-chip cloud computer processor. SIGOPS Oper. Syst. Rev. 45(1), 73–83 (2011)
15. Tim, M., van der Rob, W.: RCCE: a Small Library for Many-Core Communication. Intel Many-core Applications Research Community, document version 0.75 (September 2010)
16. Naffziger, S.: High-Performance Processors in a Power-Limited World. In: VLSI Circuits, 2006 Symposium on Digest of Technical Papers, pp. 93–97 (2006)
17. Krste, A., et al.: The Lanscape of Parallel Computing Research: A View from Berkeley, EECS techinical report (December 2006)
18. Brey, B.B.: The Intel Microprocessors 8086/8088, 80186/80188, 80286, 80386, 80486, Pentium and Pentuim Pro Processor: Architecture, Programming and Interfacing, 4th edn., ISBN: 81-203-1220-1

Solar Power Station Monitoring System with Five Remote Functions and Double Intelligent Control Loop

Dingjin Huang[1], Yunqiang Zheng[1], and Hadi Malek[2]

[1] School of Optoelectronic Engineering, Xi'an Technological University
Xi'an, 710032, China
[2] Department of Electrical & Computer Engineering, Utah State University
4120 Old Main Hill, Logan UT 84322-4120, USA
zhengyunqiang585@126.com, hdjing18@yahoo.com.cn,
hadi.malek@nceis.com

Abstract. In this paper, by using ARM Cortex-M3 embedded high-performance processor, we implement a remote monitoring system for a solar power station with five essential functions which are telemetry, remote control, remote signal, remote dispatch and remote vision. In this system, Data Acquisition Unit, Data Transmit Unit and Monitoring Centre Unit are combined to form this remote monitoring system. This remote intelligent monitoring system enables power station's operators to check the station status anytime and anywhere through the internet or cell phone, and they can send pre-defined command in the special conditions or doing supervision tasks. This system improves the monitoring system's integrity, reliability, flexibility and intellectuality.

Keywords: Five remotes, Double intelligent control loop, Remote monitoring system, Data fusion, ARM Cortex-M3.

1 Introduction

The era of fossil fuels, As a Main part of our energy supplies, is coming to the end by next some years. Then using new forms of energy instead of traditional forms of energy is necessary. Remarkable daily amount of energy from the sun, and the fact that using solar energy is free of environmental pollution and harmful gases, makes solar energy as a proper source to replace fossil Fuels. In areas where there is sufficient amount of solar energy, a solar power plant is the best way of generating electricity. Optimum use of a great permanent, endless and always available source of energy is another advantage of this energy. Nowadays, main problem of using solar power stations is high costs of establishing and operating of these stations. Among all methods suggested for solar station monitoring, those methods which contain lower costs, shorter construction time and higher reliability are more desirable.

Most application of solar power station is in the desert, grassland, basin, shallow water and other regions, where are not covered by national power grid, but these areas contain a huge resources of solar energy. Nowadays, as a part of dispatch automation system, most of solar power station monitoring systems contain data acquisition and

D. Yang (Ed.): Informatics in Control, Automation and Robotics, Volume 2, LNEE 133, pp. 27–34.
springerlink.com

monitoring function, which are isolated from other systems and they form an island of information effect in the power systems.

Moreover, current monitoring systems have only four remote functions and also the common used data processing methods add the collected information together simply or using the ballot choices, which these methods reduces the reliability and intellectuality.

In this paper, Solar Power Station Monitoring System with five remote functions and double intelligent control loop (SPSMS) is presented. SPSMS enables operator to check the station's status anytime and anywhere and increases power station safety level.

In the following, in section 2 we present the main function and proposed system configuration. Hardware and software design are described in section 3 and section 4 and finally, section 5 is conclusion.

2 System Architecture and Functions

SPSMS overall configuration is shown in Figure1.

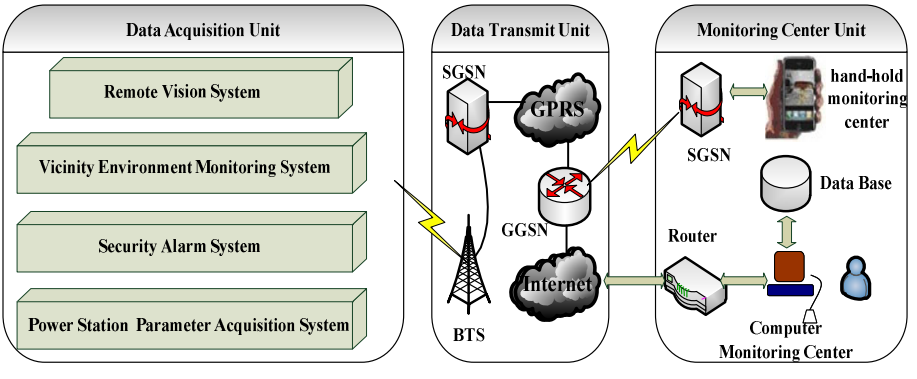

Fig. 1. SPSMS overall configuration

This system is divided into three units. First unit is data acquisition unit which is constituted by remote terminal unit (RTU) and local instruments. This unit has functions of vicinity environment monitoring, remote vision, security alarm and power station operation parameters acquisition. In this unit, Field data are collected by sensors and will be preprocessed comprehensively and intelligently. It can also communicate with the local equipments based on MODBUS communication protocol to debug or maintain them.

Second unit is data transmit unit which contains optical fiber, GSM/GPRS wireless network and Ethernet cable to realize long distance communication.

Third unit is monitoring center unit with double intelligent control loop. The primary control loop is a centralized monitoring center consisting of industrial personal computer and Web Server. It works through operating serial port or network port to realize Data analyzing, data sorting, data displaying, control instructions

sending, and so on. All of processed information will be released through TCP/IP protocol and therefore will be accessible through a designed website according to the requirements eventually. The secondary control loop is the hand-held mobile terminals. Control software is based on Wince. It can check the station's status anytime and anywhere through cell phone.

SPSMS has five remote duties including telemetry, remote control, remote signal, remote dispatch and remote vision.

3 Hardware Design

Data acquisition unit circuit configuration is shown in Figure2:

The embedded controller of SPSMS is STM32F107VC based on the ARM Cortex-M3 produced by STMicroelectronics CO. Hardware circuit can be divided into five parts which is sensor data collecting circuit, external devices communication circuit, input/output controlling circuit, security alarm circuit and network communication circuit.

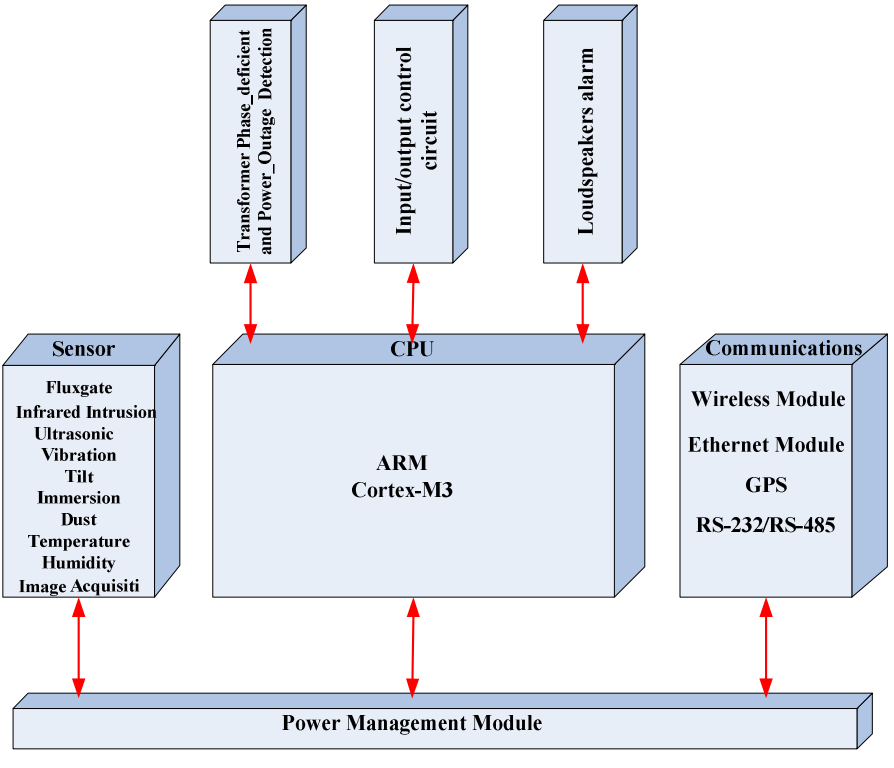

Fig. 2. Data acquisition unit circuit configuration

Sensor data collecting circuit processes sensors signals including humidity and temperature sensors, dust content sensors, water immersion sensors, vibration sensors, tilt sensors, windows state sensors, infrared intrusion sensors, ultrasonic sensors, transformer phase lack and power failure sensors. Humidity and temperature sensor communicate with the CPU via single-wire bus; other sensors can be directly connected to GPIO. Transformer phase lack and power failure sensor will produce a low voltage if there is any lack of phase in transmission line. All sensors connected to CPU are isolated by the photon coupled isolators.

External communications circuit communicates with the local equipments based on MODBUS communication protocol. This circuit is responsible for collecting local equipments data including image data, GPS geographic data, solar controller working state, current data and voltage data. Also, SPSMS enables operator to debug the equipments via the external communication circuit. Image acquisition circuit is constituted by the CMOS sensor, image acquisition module and mass storage. This circuit is designed with infrared illuminator in order to collect images in the dark condition. Image acquisition module is responsible for CMOS sensor exposure setting, image resolution setting, formats and contrast settings .The image is compressed into JPEG file format and transmits via RS485 serial port. The image will be stored in SD card. GPS module connect to CPU via RS232 serial port and produces data containing latitude, longitude, speed, direction Angle, year, month, hours, minutes, seconds, milliseconds and other information. The circuit reads the voltage, current data and the solar controller information, running state and other information from the local instruments.

Input/output controlling circuit is constituted by relay controlling unit. The circuits can control power supply, security and alarm equipments to change switch's state. The relay controlling unit adopts independent power supply mode, add the backflow inhibit circuit and electric spark suppression circuit to increase the stability and reliability.

Security alarm circuit is constituted by high-pitched loudspeakers, alarm and audio surveillance unit. It is responsible for the security, defending and audio intercepting etc. A microphone is connected to the MICO_P and MICO_N pins in the wireless communication module. High-pitched loudspeaker is connected to the SPKO_P and SPKO_N pins. If any unusual events (such as thieves broke into) happen, CPU will trigger the microphone to pick-up audio signal automatically, and open the alarm and high-pitched loudspeakers to overawe thief automatically.

Network communication circuit is constituted by Ethernet communication circuit and GSM/GPRS wireless communication circuit. It is responsible for sending the data via Ethernet and GSM/GPRS wireless network to the monitoring center and receiving the data from the monitoring centre. Specific implementation as follows:

(a) The data collected is sent to the monitoring centre by CPU through Ethernet.

(b) CPU calls AT instructions to send the data to computer monitoring centre and the hand-held monitoring center in forms of GPRS transparent transmission or the SMS/MMS mode.

4 Software Design

4.1 Communication Protocols and Data Fusion Algorithm

Communication protocol between the RTU and the computer monitoring center should be established. Data frame format can be divided into command message and response message. A detailed command message protocol format is as table1:

Table 1. Command message

SeqNr	Addr0	Addr1	Com	Len	Data[0…n]	CRC	End

SeqNr: the message head, command message serial number identification (1 byte) Addr0 Addr1: RTU address, divided into provincial address and regional address (2 bytes)

Com: the command sender command type identification (1 byte)

Len: length of data (2 bytes)

Data [0…n]: Data bytes

CRC: CRC checking (2 bytes)

End: end identification (1 byte)

A detailed response message protocol format is as table2:

Table 2. Rresponse message

SeqNr	Addr0	Addr1	Type	Len	Data[0…n]	CRC	End

SeqNr: the message head, command message serial number identification (1 byte) Addr0 Addr1: RTU address, divided into provincial address and regional address (2 bytes)

Type: the data sender data Type identification (1 byte)

Len: length of data (2 bytes)

Data [0…n]: Data bytes

CRC: CRC checking (2 bytes)

End: end identification (1 byte)

Following industrial communication standard, Modbus_RTU communication protocol is adopted between RTU and other instruments in the power station.

Using data fusion technology to improve reliability and intellectuality, prevent error and omission alarms. SPSMS determines the weights and membership functions of each sensor based on the estimation method and classical statistical method. For example, there are N sensors to measure physical quantities and the collected data from the first sensor is X_i, in which i=l, 2, …, n. SPSMS averages each sensor's data with its weighting factor W_i ($\sum_{i=0}^{n} W_i = 1$), the weighted average of the results is:

$$\overline{X} = \sum_{i=0}^{n} W_i X_i = WX \tag{1}$$

Because of different quality of each sensor and other interference factors, X_i has randomness characteristics. Suppose X_i are independent and distributed as N (μ_i,σ_i). Sensor precision can be calculated by:

$$\sigma = \frac{\sigma_i}{\sqrt{n}} \tag{2}$$

Obviously by doing this averaging process, the result data is more reliable than using individual sensor signal.

4.2 Remote Terminal Unit Software Design

The structured top-down programming method is used in the RTU software design. According to the function, system software can be divided into initialization program module, networking and data sending program, image acquisition program, SD card reading and writing program, GPS geographic data reading and writing program, sensor data collection and fusing program, short message and MMS sending program, external device communications and debugging program, input/output controlling program, terminal services program and the main program.

The main program sets the configuration of the I/O pins, timer, registers, and USART after power on. Then calls instruction to complete GPS module, camera module, Peripheral modules to initialize, and defines ring buffer array FIFO and the frame format of the upload data.

The main program coordinates and controls the subprogram through the timer interruption, external interruption and USART interruption. The image acquisition program uses USART DMA mode in the image data acquisition. Reading and writing data will be controlled by the DMA controller instead of interruption. Thus the efficiency can be greatly improved. The main program flow diagram is shown in Figure3:

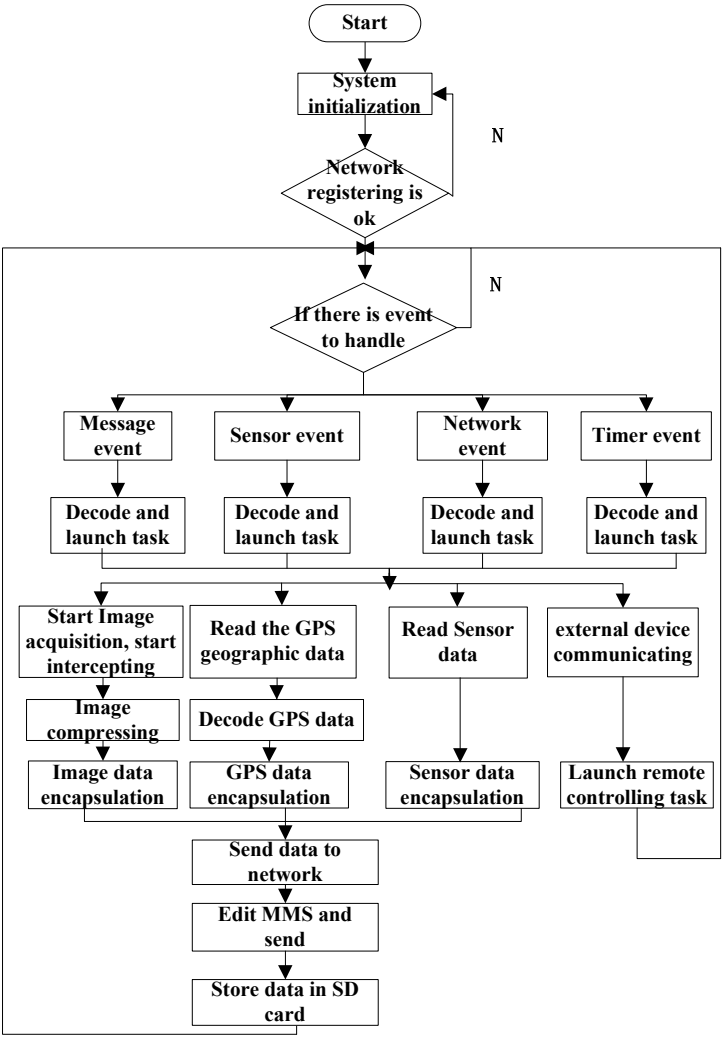

Fig. 3. The main program flow diagram

4.3 Monitoring Centre Software Design

According to the function, the monitoring software can be divided into three subprograms: Data transmission and analyzing section, database section, and data display section. The whole software is C/S structure. Socket operation receives and decodes the data, then saves the effective data SQL. The data will be released as a WEB form, which enables the user to search conveniently. TCP/IP protocol is used in the monitoring centre. SQL database servers accept client request, return processed results or middle data to the client. Also, SQL database serve as the centre of the system controlling, maintenance, analyzing, and data statistics. The real-time state of

the power station will be displayed on the monitoring centre. Any emergency will be displayed immediately. The alarm information includes alarm level, location, time and other information.

5 Conclusion

By using high-performance embedded ARM Cortex-M3 processor, this paper design a remote monitoring system constituted by data acquisition unit, data transmit unit and monitoring center unit to form, and realize unattended solar power station monitoring with five remotes and double intelligent control loop.

There are two innovations in this system:

(a) SPSMS overcomes the islanding effect in the solar power station monitoring system, forms measurement and control system with organic relationship. When emergency happens, system has a nice dynamic linkage. Functions of remote dispatch and remote vision will improve the modernization of the solar power station monitoring system.

(b) SPSMS is designed with double intelligent control loop that enable operator to check the station status anytime and anywhere. Data fusion technology is used to reduce the error and omission alarms. This system improves the monitoring system's integrity, reliability, flexibility and intellectuality.

References

1. Flores, A., Sáez, D.: Fuzzy Predictive Control of a Solar Power Plant, pp. 58–66. IEEE Press (2005)
2. Kang, D.-J., Kim, H.-M.: Development of test-bed and security devices for SCADA communication in electric power system. In: 2009 Telecommunications Energy Conference (2009)
3. Yang, J., Jia, X.: Study Of Image Recognition Used For Unattended Substation. Master's Thesis of North China Electric Power University, D.BeiJing (2004)
4. Varshney, P.K.: Multisensor data fusion. Electronics & Communication Engineering Journal 12, 245–253 (1997)
5. Foresti, G.L.: A real-time system for video surveillance of unattended outdoor environments Circuits and Systems for Video Technology. IEEE Transactions 8(6), 697–704 (1998)
6. Itschner, R., Pommerell, Rutishauser, M.: Remote monitoring of embedded systems in power Engineering. IEEE Internet Computing (1998)
7. Andrea, A., Casini, A.L.: Embedded Java in a web-based teleradiology system. IEEE Internet Computing 2(3), 60–68 (1998)

Design of Portable Solar Energy System with Fast-Stationed Feature

Dingjin Huang and Yanwu Ma

School of Optoelectronic Engineering, Xi'an Technological University
Xi'an, China, 710032
jiao_251406174@qq.com

Abstract. He article had designed a portable solar energy system with fast-stationed feature. The system uses CAN-Bus and the parallel and sharing current technology that enables the system to achieve a distributed redundant expansion and rapidly set up power stations. The system is able to offer power to equipment on the environment without electricity environments, such as the outdoor travel, scientific investigation and field working ones. By the way, power station organized fast can meet the long-term, high-power power supply needs on field condition.

Keywords: Fast-stationed, Portable system, CAN-Bus, MPPT.

1 Introduction

In travel, scientific exploration or field work condition, people often use batteries, portable solar power, generators and other equipments to offer power to electrical equipment. Portable solar power device, due to its technical conditions, it is difficult to achieve high-capacity, high power output requirements, unable to meet the complex application environment and load demand.

Development of power system is a distributed power system instead of centralized power supply system. Compared the collective power system, distributed power system has more advantages: increased flexibility of the system; higher the module's power density lead to small size and height; improved system reliability because the electrical stress of the power semiconductor device in each module has been reduced; easier redundant expansion due to a distribution system; easier standardization due to small range.

The portable solar energy system with fast-stationed feature adopts distribution design, can enlarge the capacity and output power of system. The portable solar energy system had achieved the management of power in the station with CAN-Bus, and adjusted the parallel and sharing current with parallel and sharing unit in order to decrease the system damage and ensure the system stable outputting.

D. Yang (Ed.): Informatics in Control, Automation and Robotics, Volume 2, LNEE 133, pp. 35–40.
springerlink.com

2 The Overall Design of the System

2.1 Design of System Perform

The portable solar energy system with fast organized feature begins with aims that being portable, being fast charging, multi-output, and redundant expansion .In order to make full use of electricity power transited from solar energy , the MPPT technology and the charging method of approximation of ideal charge curve is used in the charging unit of this system. The power output unit of this system consists of the isolated DC / DC conversion circuit and DC / AC inverter circuit to increase the output power. Besides, this system has expansion feature, which allows a single portable system of solar cells and energy storage unit to expand. At same time, this system adopts CAN-Bus technology and the parallel and sharing current technology, enabling the system to achieve the expansion of distributed redundancy which makes N +1 portable system form into a series-parallel connected solar power station.

2.2 System Composition

PV module changes solar energy into electrical energy. In under the control of the controller, MPPT charging unit automatic tracks the PV maximum power point, adjusts the voltage of the PV module output, charges up energy storage unit. The voltage of Energy storage unit output goes through DC/DC adjusting circuit or DC/AC inverter circuit to supply DC or AC load. Operation parameters of each unit were collected by the controller, and displayed in the LCD monitor. Then, the controller intelligent controls the operation status of each unit. A number of systems can organize a solar power station through the CAN-Bus network. The system frame shown in figure 1.

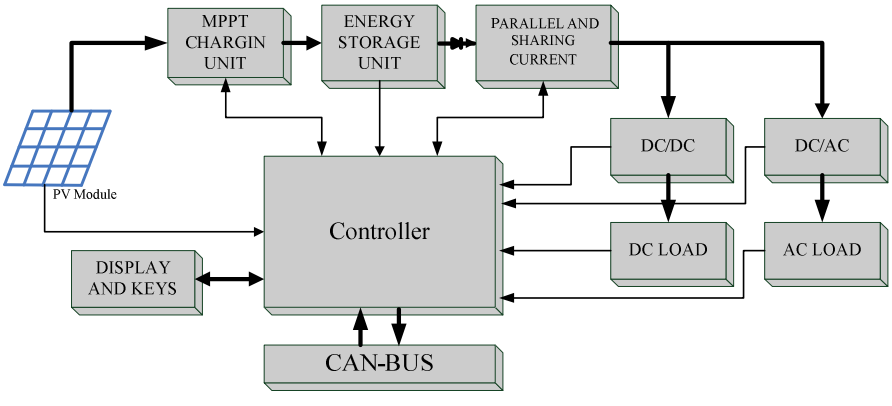

Fig. 1. The frame of portable solar energy system with fast organized feature

The microprocessor with ARM Cortex-M3 core was used in the system. The system has the functions of data acquisition, data storage, intelligent control, over voltage, over charge, over discharge, reverse polarity protection, alarm and display.

MPPT Charging Unit: It can track maximum power point of the solar cell, and complete the charging function.

Energy Storage Unit: It uses a modular design, the battery is made into the energy storage module, which can be easily demolished and replaced. It can be used a backup power.

DC / DC: It adjusts the direct voltage of the battery output to supply voltage to DC loads.

DC / AC: It transforms the direct voltage into alternating current voltage, then supplies AC load.

Parallel and Sharing Unit: it adjusts the current of the system output, reduce the difference of each portable system output current when they are used to from a power station.

CAN-Bus: In the formation of power station, we can establish local area communications network with CAN-Bus, manage electric quantity of each portable systems in the power station with distributed. CAN-Bus is the premise to achieve system redundancy, and rapid formation of power station.

3 CAN-Bus

3.1 The Application of CAN-Bus in Portable System

It is told that CAN is a short call for Controller Area Network. CAN-Bus nodes on the network can actually reach 112 to meet the need of organizing distribution and redundant expansion station.

CAN-Bus is a connection of managing the power distribution between several portable systems. CAN-Bus makes a whole power web, using several portable systems. Each system makes a communication with others with CAN-Bus. When one portable system is lack of power, CAN-Bus cut off the one or the branch of this system so that the power station can work normally. Not the system does get access to the station until the offering power condition of this system is conformed.

3.2 CAN-Bus Communication Circuit

With fast combine-station function, the CAN-Bus communication circuit of solar portable system shown in figure 2, MCU's serial data input and output connect CAN-Bus transceiver MCP2551 with high-speed optical isolated devices TLP113. In order to enhance anti-jamming capability of CAN node, using both ends of the TLP113 isolated power supply, produce a isolated CAN 5V signal by DC-DC devices, while the power supply of input +5V and STM32 is in common ground. In order to reduce the device's radio frequency interference, MCP2551'RS side grounded through resistance, turn the MCP2551 into the slope-control mode, reduce the output current of the RS side, thereby limiting the CANH and CANL rise and fall times, and further reduce EMI. In order to filter out high frequency interference on the bus, to prevent

electromagnetic radiation, in the MCP2551 CANH and CANL side grounded through 30pF capacitors. In order to protect MCP2551 against over-current impact, series connect a 5Ω resistor between each side of CANH and CANL with bus to limit current. In order to impedance matching with cable and ensure the data signals would not reflected at both ends of bus, connect a 120Ω resistor between CANH and CANL, which is defined in ISO11898 linear topology rating resistance at both ends of bus.

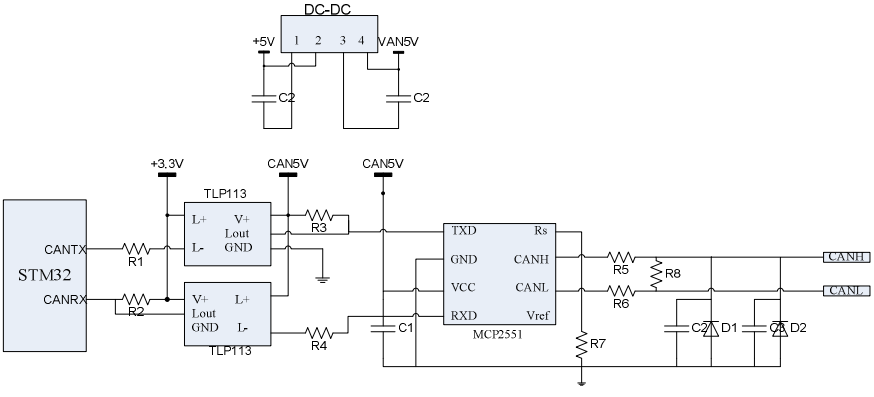

Fig. 2. CAN-Bus communication circuit

4 Parallel and Sharing Unit

4.1 Parallel and Sharing Current Technology

In the development of the switching power supply the parallel and sharing current technology is proposed. The bias existed in parameters and changes caused by operating environment will lead to the current distributed not evenly. Some of the output current is large and some is small while the others does not have the output. The switch in the power module which shares more current will have thermal stress augment. The system reliability therefore is reduced and the working life of the power module is shorter or the module may be damaged that can not maintain the normal work.

Parallel and sharing current technology enables the power modules which are working in parallel share the load current evenly. The current in this case is called load current sharing. The role that the load current sharing plays is to make sure that each module in the system can output power effectively and in the best working condition ensuring that the power system is stable, reliable, and efficient. Parallel current sharing technology makes the power systems flexible to expand its capacity. The power system has a very high serviceability once a single power supply module fails it can be easily hot-swap replaced or repaired.

4.2 Method OF Parallel AND Sharing Current

The common used methods of Parallel and sharing current are: the output impedance, master-slave setting, the average current automatic sharing current, the maximum current automatic sharing current and so on.

Though the parallel DC module has many solutions to carry out the current sharing, while as for the distributed solar electric power, there will be more or less defectives that lead to the output impedance of current-sharing accuracy is not very high. Master set method and the average current laws can not achieve redundancy, the maximum current automatic current sharing law is better. However, all the three methods are the hardware current sharing program which has many problems in current sharing such as the high cost, hard to change and to expand. Aiming at that, this paper proposed a software current sharing plan. Software current sharing method possesses a convenient, low cost, easy to change and upgrade features.

Software current sharing method is to collect the output current of each portable system and then calculate the total output current of the power station. The average output current of each portable system is calculated according to the number of the portable system. Then, the system according to current sharing requirements, compared to the unit's output current, adjustable output current of the unit, ensure that the current offset within the scope and conduct a continuous comparison of the current continued to promote the approximation of each module, each module to achieve balance between the output current, achieve parallel and sharing current.

5 Conclusion and Outlook

Distributed power systems instead of centralized power supply system is one of the power system development, and distributed solar power generation systems have enabled the solar energy toward the distributed development , The portable solar energy system with fast-stationed feature will be one of solar power systems' design development direction. The application of CAN-Bus technology and Parallel and sharing current technology enable portable system flexibly realize redundant expansion, improve the system limitations of portable solar power current application, which make portable solar energy systems have a wider range of applications.

References

1. Zhang, L., Huang, Z., Liu, C., et al.: Experimental Study on Parallel Connecting of MOSFETs. Telecom Power Technologies 6, 5–7 (2007)
2. Jiang, J.-A., Huang, T.-L., Hsiao, Y.-T., Chen, C.-H.: Maximum Power Tracking for Photovoltaic Power Systems. Tamkang Journal of Science and Engineering 8(2), 147–153 (2005)
3. Sun, Q., Wang, X., Gao, Y.: Study of the Current Balance of IGBTs in Paralleling. Power ElectronicTechnology 38(1), 4–6 (2002)
4. Zhang, Z., Shen, H., Chen, W., Shu, J.: The Design and Performance of Portable Integrated PV System. In: The 8th PV Conference Proceedings, pp. 612–616 (2004)

5. Zhang, S., Xiang, L., Yao, G.: Controlling Means of Parallel Current Sharing in Blocking DC Power Supply. World Power Supply, 12–15 (2007)
6. Shi, J., Shan, C., Tong, H., Fang, P.: Solar Cell MPPT Controller based on MCU. Power Electronics 42(11), 45–46 (2008)
7. Lu, L., Zhang, S., Shu, G.: Research on Max Power Point Tracking for Solar-Electric Charging System based on Micro-Controller. Power Electronics 41(2), 96–98 (2007)
8. Xiao, W., Dunford, W.G.: A Modified Adaptive Hillclimbing MPPT Method for Photovoltaic Power Systems. In: IEEE PESC 2004, vol. (3), pp. 195–196 (2004)
9. Ai, B., Yang, H., Shen, H., Liao, X.: Computer-aided design of PV/Wind hybrid system. Renewable Energy 28, 1491–1512 (2003)
10. Lin, X.: Power Electronic Technology. Tsinghua University Press (2009)

The Fuzzy Binary Relations on n- Frustum Pyramid Fuzzy Number Space and Its Application

Jiaxi Zhang, Guixiang Wang, and Jie Du

Institute of Operational Research and Cybernetics
Hangzhou Dianzi University, Hangzhou, 310018, China
mathdogged@126.com

Abstract. In this paper, we give a definition of n – frustum pyramid fuzzy numbers (a kind of n – dimensional fuzzy numbers which is easy to be used). And we define two fuzzy binary relations on n – frustum pyramid fuzzy number space according to the characteristics of the special fuzzy numbers, study its properties. And then, we infer the computational formula which is easy to be programmed. At last we give a practical example to show the application in classification which is based on fuzzy approximation relation on n – frustum pyramid fuzzy numbers space.

Keywords: fuzzy numbers, n – frustum pyramid fuzzy numbers, fuzzy approximation relation, classification.

1 Introduction

The concept of fuzzy set was first put forward by Zadeh in 1965 [1], and Chang and Zadeh proposed the concept of fuzzy numbers in 1972 [2]. With the development of mathematics, more and more researchers studied the properties and applications of fuzzy numbers to meet the engineering research. In 2002, Wang [3] introduced the concept of fuzzy n – cell numbers. In 2007, Wang proved that fuzzy n – cell numbers and n – dimensional fuzzy vectors can represent each other [4]. Afterward, Wang studied the ranking, pattern recognition and classification in an imprecise or uncertain environment based on fuzzy n – cell numbers [5].

Compared with general fuzzy numbers, fuzzy n – cell number has possessed of satisfying properties, which provide some convenience in both theory and application. However, its calculation in application is somewhat complicated. Therefore, we propose a special kind of n – dimensional fuzzy numbers which is easy to be calculated, namely n – frustum pyramid fuzzy number. We define two fuzzy binary relations on n – frustum pyramid fuzzy number space according to the characteristics of the special fuzzy numbers, study its properties. And then, we infer the computational formula which is easy to be programmed. At last we give a practical example to show the application in classification which is based on fuzzy approximation relation on n – frustum pyramid fuzzy numbers space.

D. Yang (Ed.): Informatics in Control, Automation and Robotics, Volume 2, LNEE 133, pp. 41–48.
springerlink.com

2 Basic Definitions and Notations

Fuzzy sets defined in R^n ($n-$ dimensional Euclidean Space) is a function. $u: R^n \to [0,1]$. For each such fuzzy set u, we denote by $[u]^r = \{x \in R^n : u(x) \geq r\}$ for any $r \in (0,1]$, we name it the $r-$level of fuzzy set u. The definition of the support of fuzzy set u is $\{x \in R^n : u(x) > 0\}$. Then, $[u]^0 = \overline{\{x \in R^n : u(x) > 0\}}$. Fuzzy number is a special fuzzy set which should meet the following four conditions: u is normal; u is fuzzy convex; $u(x)$ is upper semi-continuous; $[u]^0$ is a compact set. Let E^n denote the collection of all fuzzy sets of R^n. If $u \in E^n$, and $[u]^r$ can be represented by $\prod_{i=1}^{n}[\underline{u_i}(r), \overline{u_i}(r)]$, $\forall r \in [0,1]$, where $\underline{u_i}(r) \leq \overline{u_i}(r)$, ($i = 1,2,\cdots,n$), then we call u a fuzzy $n-$cell number. And, we denote the collection of all fuzzy $n-$cell numbers by $L(E^n)$. If $u \in E$, and there exist $a,b,c,d \in R$ with $a \leq b \leq c \leq d$ such that

$$u(x) = \begin{cases} \dfrac{x-a}{b-a}, & if \quad x \in [a,b] \\ 1, & if \quad x \in [b,c] \\ \dfrac{x-d}{c-d}, & if \quad x \in [c,d] \\ 0, & if \quad x \notin [a,d] \end{cases}$$

Then u is called a trapezoidal fuzzy number and denoted as $u = (a,b,c,d)$. If $b = c$, u is a triangle fuzzy number, $u = (a,b,d)$.

Let $u_i \in E$, ($i = 1,2,\cdots,n$), $n-$dimensional fuzzy vector is refer to ordered group with n elements as $u = (u_1, u_2, \cdots, u_n)$. In [4], it is proved that fuzzy $n-$cell numbers and $n-$dimensional fuzzy vectors can represent each other. So, for any $u \in L(E^n)$, we can represent it as a vector.

Let $u = (u_1, u_2, \cdots, u_n) \in L(E^n)$, $v = (v_1, v_2, \cdots, v_n) \in L(E^n)$, $\alpha = (\alpha_1, \alpha_2, \cdots, \alpha_n) \in R^n$, and α satisfies $\sum_{i=1}^{n} \alpha_i = 1, \alpha_i \geq 0$, ($i = 1,2,\cdots,n$). Let $M_\alpha(u) = \sum_{i=1}^{n} \alpha_i \int_0^1 r[\underline{u_i}(r) + \overline{u_i}(r)]dr$,

$D_\alpha(u) = \sum_{i=1}^{n} \alpha_i [\overline{u_i}(r) - \underline{u_i}(r)]dr$, then we call $M_\alpha(u)$ and $D_\alpha(u)$ the weighted mean and the weighted fuzzy degree respectively. $\rho_\alpha(u,v)$ is a metric between u and v, and $\rho_\alpha(u,v) = \sum_{i=1}^{n} \alpha_i \int_0^1 r[\left|\underline{u_i}(r) - \underline{v_i}(r)\right| + \left|\overline{u_i}(r) - \overline{v_i}(r)\right|]$. Define $u \leq v$ if and only if $\underline{u_i}(r) \leq \underline{v_i}(r)$ and $\overline{u_i}(r) \leq \overline{v_i}(r)$, ($i = 1,2,\cdots,n$), $\forall r \in [0,1]$.

3 Fuzzy Binary Relations

Definition 1. Let $u = (u_1, u_2, \cdots, u_n) \in L(E^n)$. If $u_1, u_2, \cdots, u_n$ are all trapezoidal fuzzy numbers, then we call u a $n-$frustum pyramid fuzzy number. And if $u_i = (a_i, b_i, c_i, d_i)$, ($i = 1,2,\cdots,n$), then we denote u by

$$u=\begin{pmatrix} a_1 & a_2 & \cdots & a_n \\ b_1 & b_2 & \cdots & b_n \\ c_1 & c_2 & \cdots & c_n \\ d_1 & d_2 & \cdots & d_n \end{pmatrix}$$

And we denote the $n-$ frustum pyramid fuzzy number space by $FP(E^n)$. If $b_i=c_i$, ($i=1,2,\cdots,n$), u is a $n-$ pyramid fuzzy number.

Lemma 1. Let $u\in FP(E^n)$, $v\in FP(E^n)$, $u_i=(a_i,b_i,c_i,d_i)$, $v_i=(a_i',b_i',c_i',d_i')$, ($i=1,2,\cdots,n$).

(1). $u\le v \Leftrightarrow a_i\le a_i'$, $b_i\le b_i'$, $c_i\le c_i'$, $d_i\le d_i'$, $(i=1,2,\cdots,n)$, $\forall r\in[0,1]$.

(2). $u\subset v \Leftrightarrow a_i'\le a_i$, $b_i'\le b_i$, $c_i\le c_i'$, $d_i\le d_i'$, $(i=1,2,\cdots,n)$, $\forall r\in[0,1]$.

Theorem 1. $\forall u\in FP(E^n)$, $\alpha=(\alpha_1,\alpha_2,\cdots,\alpha_n)\in R^n$, and $\sum_{i=1}^n\alpha_i=1,\alpha_i\ge 0$ $(i=1,2,\cdots,n)$.

$$M_\alpha(u)=\frac{1}{6}\sum_{i=1}^n\alpha_i(a_i+d_i)+\frac{1}{3}\sum_{i=1}^n\alpha_i(b_i+c_i)\ ,\ D_\alpha(u)=\frac{1}{6}\sum_{i=1}^n\alpha_i(d_i-a_i)+\frac{1}{3}\sum_{i=1}^n\alpha_i(c_i-b_i)$$

Proof. It is easy to know $\underline{u_i}(r)=(b_i-a_i)r+a_i$, $\overline{u_i}(r)=(c_i-d_i)r+d_i$. So, we have

$$\begin{aligned} M_\alpha(u)&=\sum_{i=1}^n\alpha_i\int_0^1 r[\underline{u_i}(r)+\overline{u_i}(r)]dr \\ &=\sum_{i=1}^n\alpha_i\int_0^1 r[(b_i-a_i)r+a_i+(c_i-d_i)r+d_i]dr \\ &=\sum_{i=1}^n\alpha_i[(a_i+d_i)\int_0^1 rdr+(b_i+c_i-a_i-d_i)\int_0^1 r^2dr] \\ &=\sum_{i=1}^n\alpha_i[\frac{a_i+d_i}{2}+\frac{b_i+c_i-a_i-d_i}{3}] \\ &=\frac{1}{6}\sum_{i=1}^n\alpha_i(a_i+d_i)+\frac{1}{3}\sum_{i=1}^n\alpha_i(b_i+c_i) \\ D_\alpha(u)&=\sum_{i=1}^n\alpha_i\int_0^1 r[\overline{u_i}(r)-\underline{u_i}(r)]dr \\ &=\sum_{i=1}^n\alpha_i\int_0^1 r[((c_i-d_i)r+d_i)-((b_i-a_i)r+a_i)]dr \\ &=\sum_{i=1}^n\alpha_i[(d_i-a_i)\int_0^1 rdr+(a_i+c_i-b_i-d_i)\int_0^1 r^2dr] \\ &=\sum_{i=1}^n\alpha_i[\frac{d_i-a_i}{2}+\frac{a_i+c_i-b_i-d_i}{3}] \\ &=\frac{1}{6}\sum_{i=1}^n\alpha_i(d_i-a_i)+\frac{1}{3}\sum_{i=1}^n\alpha_i(c_i-b_i) \end{aligned}$$

Theorem 2. $u,v\in FP(E^n)$, then

$$\rho_\alpha(u,v)=\sum_{i=1}^n\alpha_i\int_0^1 r\{\left|[(b_i-a_i)-(b_i'-a_i')]r+a_i-a_i'\right|+\left|[(c_i-d_i)-(c_i'-d_i')]r+d_i-d_i'\right|\}dr$$

Definition 2. Let $u,v\in FP(E^n)$, $p\in[0,1]$, $\alpha=(\alpha_1,\alpha_2,\cdots,\alpha_n)\in R^n$, and $\sum_{i=1}^n\alpha_i=1$, $\alpha_i\ge 0$, $(i=1,2,\cdots,n)$. Let $d_{\alpha,p}(u,v)=p(M_\alpha(u)-M_\alpha(v))^2+(1-p)(D_\alpha(u)-D_\alpha(v))^2$.

Definition 3. $p \in [0,1]$, we define two fuzzy binary relations on $FP(E^n)$ as follows:

$$G_{\alpha,p}(u,v) = \frac{1}{1+\sqrt{d_{\alpha,p}(u,v)}}, \quad H_{\alpha,p} = \frac{1}{1+\sqrt{p\rho_\alpha{}^2(u,v)+(1-p)[\sum_{i=1}^n \alpha_i |D(u_i)-D(v_i)|]^2}}$$

And we call the fuzzy binary relations $G_{\alpha,p}$ and $H_{\alpha,p}$ fuzzy approximation relations.

Theorem 3. $\forall u,v \in FP(E^n)$, $\alpha = (\alpha_1,\alpha_2,\cdots,\alpha_n) \in R^n$, and α satisfies $\sum_{i=1}^n \alpha_i = 1$, $\alpha_i \geq 0$, $i = 1,2,\cdots,n$.

(1). $d_{\alpha,p}(u,u) = 0$.

(2). $d_{\alpha,p}(u,v) = d_{\alpha,p}(v,u)$.

(3). $d_{\alpha,p}(ku,kv) = k^2 d_{\alpha,p}(u,v)$.

Proof. Obviously, (1) and (2) are right. So we only show (3). According to the definition of $M_\alpha(u)$ and $D_\alpha(u)$, we know $M_\alpha(ku) = kM_\alpha(u), D_\alpha(ku) = |k| D_\alpha(u)$. So we have $d_{\alpha,p}(ku,kv) = p(kM_\alpha(u) - kM_\alpha(v))^2 + (1-p)(|k|D_\alpha(u) - |k|D_\alpha(v))^2 = k^2 d_{\alpha,p}(u,v)$.

Remark 1. $d_{\alpha,p}(u,v) + d_{\alpha,p}(v,w) \geq d_{\alpha,p}(u,w)$ is not necessarily true, so $d_{\alpha,p}$ is not a metric.

Theorem 4. $\forall u,v \in FP(E^n)$, $\alpha = (\alpha_1,\alpha_2,\cdots,\alpha_n) \in R^n$ and $\sum_{i=1}^n \alpha_i = 1, \alpha_i \geq 0$.

$$d_{\alpha,p}(u,v) = \frac{p}{36}\{\sum_{i=1}^n [(a_i - a_i') + 2(b_i - b_i') + 2(c_i - c_i') + (d_i - d_i')]\}^2$$
$$+ \frac{1-p}{36}\{\sum_{i=1}^n [(a_i' - a_i) + 2(b_i' - b_i) + 2(c_i - c_i') + (d_i - d_i')]\}^2$$

Proof. According to Theorem 1, we can get the formula easily.

Deduction 1. If u,v are $n-$ pyramid fuzzy numbers, i.e. $b_i = c_i, b_i' = c_i'$ then

$$d_{\alpha,p}(u,v) = \frac{p}{36}\sum_{i=1}^n [(a_i - a_i') + 4(b_i - b_i') + (d_i - d_i')]^2 + \frac{1-p}{36}\sum_{i=1}^n [(a_i' - a_i) + (d_i - d_i')]^2$$

Theorem 5. $\forall u,v \in FP(E^n)$, $\alpha = (\alpha_1,\alpha_2,\cdots,\alpha_n) \in R^n$, and $\sum_{i=1}^n \alpha_i = 1, \alpha_i \geq 0$.

(1). $v \leq u \Rightarrow \rho_\alpha(u,v) = M_\alpha(u) - M_\alpha(v)$.

(2). $v \subset u \Rightarrow \rho_\alpha(u,v) = \frac{1}{6}\sum_{i=1}^n \alpha_i (a_i' - a_i + d_i - d_i') + \frac{1}{3}\sum_{i=1}^n \alpha_i (b_i' - b_i + c_i - c_i')$.

Proof. According to the definition of $v \leq u$, we know $a_i' - a_i \leq 0$, $b_i' - b_i \leq 0$, $c_i' - c_i \leq 0$, $d_i' - d_i \leq 0$, $(i = 1,2,\cdots,n)$, $\forall r \in [0,1]$.

Let $f(r) = [(b_i - b_i') - (a_i - a_i')]r + a_i - a_i'$, it is easy to know $f(0) \geq 0$, $f(1) \geq 0$, and the function $f(r)$ is either monotonically nonincreasing function, or monotonically nondecreasing function. Therefore, we know $f(r) \geq 0$, $\forall r \in [0,1]$. Simultaneously, Let $g(r) = [(c_i - c_i') - (d_i - d_i')]r + d_i - d_i'$, we get $g(r) \geq 0$, $\forall r \in [0,1]$. So, we have

$$\begin{aligned}\rho_\alpha(u,v) &= \sum_{i=1}^n \alpha_i \int_0^1 r\{\left|[(b_i-a_i)-(b_i'-a_i')]r+a_i-a_i'\right|+\left|[(c_i-d_i)-(c_i'-d_i')]r+d_i-d_i'\right|\}dr \\ &= \sum_{i=1}^n \alpha_i \int_0^1 r\{[(b_i-a_i)-(b_i'-a_i')]r+a_i-a_i'+[(c_i-d_i)-(c_i'-d_i')]r+d_i-d_i'\}dr \\ &= \sum_{i=1}^n \alpha_i \int_0^1 r\{[(b_i-a_i)r+a_i+(c_i-d_i)r+d_i]-[(b_i'-a_i')r+a_i'+(c_i'-d_i')r+d_i']\}dr \\ &= \sum_{i=1}^n \alpha_i \int_0^1 r[\underline{u_i}(r)+\overline{u_i}(r)]dr-\sum_{i=1}^n \alpha_i \int_0^1 r[\underline{v_i}(r)+\overline{v_i}(r)]dr \\ &= M_\alpha(u)-M_\alpha(v)\end{aligned}$$

(2). According to the definition of $v \subset u$, we know $a_i'-a_i \geq 0$, $b_i'-b_i \geq 0$, $c_i'-c_i \leq 0$, $d_i'-d_i \leq 0$, ($i=1,2,\cdots,n$), $\forall r \in [0,1]$. Let $h(r)=[(b_i-b_i')-(a_i-a_i')]r+a_i-a_i'$. From (1), we know $h(r) \leq 0$, $\forall r \in [0,1]$. Therefore, we have

$$\begin{aligned}\rho_\alpha(u,v) &= \sum_{i=1}^n \alpha_i \int_0^1 r\{\left|[(b_i-a_i)-(b_i'-a_i')]r+a_i-a_i'\right|+\left|[(c_i-d_i)-(c_i'-d_i')]r+d_i-d_i'\right|\}dr \\ &= \sum_{i=1}^n \alpha_i \int_0^1 r\{[-(b_i-a_i)+(b_i'-a_i')]r-a_i+a_i'+[(c_i-d_i)-(c_i'-d_i')]r+d_i-d_i'\}dr \\ &= \sum_{i=1}^n \alpha_i [\frac{(a_i'-a_i)+(d_i-d_i')}{2}+\frac{(a_i-a_i')+(b_i'-b_i)+(c_i-c_i')+(d_i'-d_i)}{3}] \\ &= \frac{1}{6}\sum_{i=1}^n \alpha_i(a_i'-a_i+d_i-d_i')+\frac{1}{3}\sum_{i=1}^n \alpha_i(b_i'-b_i+c_i-c_i')\end{aligned}$$

Theorem 6. $\forall u,v \in FP(E^n)$, $p=1$, $\alpha=(\alpha_1,\alpha_2,\cdots,\alpha_n) \in R^n$, and $\sum_{i=1}^n \alpha_i=1, \alpha_i \geq 0$, $(i=1,2,\cdots,n)$. If $v \leq u$ or $u \leq v$, we can get $G_{\alpha,p}(u,v)=H_{\alpha,p}(u,v)$.

Proof. According to Theorem 5, we know if $v \leq u$, then $\rho_\alpha(u,v)=M_\alpha(u)-M_\alpha(v)$. In the same way, if $u \leq v$, then $\rho_\alpha(u,v)=M_\alpha(v)-M_\alpha(u)$. Therefore, we have

$$G_{\alpha,p}(u,v)=\frac{1}{1+\sqrt{p}\left|M_\alpha(u)-M_\alpha(v)\right|}=\frac{1}{1+\sqrt{p}\rho_\alpha(u,v)}=H_{\alpha,p}(u,v).$$

Theorem 7. $\forall u,v,w \in FP(E^n)$, $\alpha=(\alpha_1,\alpha_2,\cdots,\alpha_n) \in R^n$, and α satisfies $\sum_{i=1}^n \alpha_i=1$, $\alpha_i \geq 0$, $(i=1,2,\cdots,n)$. $w=(w_1,w_2,\cdots,w_n)$, $w_i=(a_i'',b_i'',c_i'',d_i'')$.

(1). $G_{\alpha,p}(u,u)=1$.

(2). $G_{\alpha,p}(u,v)=G_{\alpha,p}(v,u)$.

(3). $G_{\alpha,p}(u+w,v+w)=G_{\alpha,p}(u,v)$.

(4). $\frac{1}{G_{\alpha,p}(ku,kv)}=\frac{|k|}{G_{\alpha,p}(u,v)}+1-|k|$.

Proof. It is obviously that (1) and (2) hold.
(3). According to Theorem 1, we know

$$M_\alpha(u+w)=\frac{1}{6}\sum_{i=1}^n \alpha_i(a_i+d_i+a_i''+d_i'')+\frac{1}{3}\sum_{i=1}^n \alpha_i(b_i+c_i+b_i''+c_i'')$$

$$D_\alpha(u+w)=\frac{1}{6}\sum_{i=1}^n \alpha_i(d_i-a_i+d_i''-a_i'')+\frac{1}{3}\sum_{i=1}^n \alpha_i(c_i-b_i+c_i''-b_i'')$$

$$M_\alpha(v+w)=\frac{1}{6}\sum_{i=1}^{n}\alpha_i(a_i'+d_i'+a_i''+d_i'')+\frac{1}{3}\sum_{i=1}^{n}\alpha_i(b_i'+c_i'+b_i''+c_i'')$$

$$D_\alpha(v+w)=\frac{1}{6}\sum_{i=1}^{n}\alpha_i(d_i'-a_i'+d_i''-a_i'')+\frac{1}{3}\sum_{i=1}^{n}\alpha_i(c_i'-b_i'+c_i''-b_i'')$$

So we have

$$M_\alpha(u+w)-M_\alpha(v+w)=M_\alpha(u)-M_\alpha(v),\quad D_\alpha(u+w)-D_\alpha(v+w)=D_\alpha(u)-D_\alpha(v).$$

And then $d_{\alpha,p}(u+w,v+w)=d_{\alpha,p}(u,v)$. Combined with Definition 3, (3) is proved.

(4).By $d_{\alpha,p}(ku,kv)=k^2 d_{\alpha,p}(u,v)$, then,

$$G_{\alpha,p}(ku,kv)=\frac{1}{1+\sqrt{d_{\alpha,p}(ku,kv)}}=\frac{1}{1+|k|\sqrt{d_{\alpha,p}(u,v)}},$$

Then, $\frac{1}{G_{\alpha,p}(ku,kv)}-1=|k|(\frac{1}{G_{\alpha,p}(u,v)}-1)$, i.e. $\frac{1}{G_{\alpha,p}(ku,kv)}=\frac{|k|}{G_{\alpha,p}(u,v)}+1-|k|$.

4 The Application of Fuzzy Approximation Relation

In the following, we give a practical example to show the application in classification which is based on fuzzy approximation relation on $n-$ frustum pyramid fuzzy numbers.

Suppose there be four kinds of flowers, A, B, C, D. There are four characteristic, length of the calyx, width of the calyx, length of the petal, width of the petal. We want to classify A, B, C, D into two classes based on the four characteristic. There are twenty samples for each kind of flower. The data is in the following matrixes. The row and the array of each matrix represent the characteristic of the flowers and the samples, respectively.

A:
$$\begin{pmatrix}
5.02 & 4.75 & 4.73 & 4.65 & 5.08 & 5.35 & 4.65 & 5.07 & 4.49 & 4.95 & 5.45 & 4.84 & 4.85 & 4.35 & 5.15 & 5.25 & 5.28 & 5.13 & 5.72 & 5.13\\
3.55 & 3.15 & 3.25 & 3.29 & 3.52 & 3.85 & 3.34 & 3.45 & 2.94 & 3.35 & 3.45 & 3.44 & 3.02 & 3.05 & 4.13 & 4.42 & 3.99 & 3.56 & 3.85 & 3.83\\
1.35 & 1.45 & 1.35 & 1.63 & 1.44 & 1.75 & 1.35 & 1.49 & 1.53 & 1.54 & 1.55 & 1.65 & 1.42 & 1.15 & 1.27 & 1.55 & 1.36 & 1.49 & 1.75 & 1.55\\
0.21 & 0.18 & 0.23 & 0.31 & 0.21 & 0.29 & 0.33 & 0.20 & 0.21 & 0.19 & 0.30 & 0.20 & 0.17 & 0.14 & 0.20 & 0.24 & 0.28 & 0.31 & 0.25 & 0.30
\end{pmatrix}$$

B:
$$\begin{pmatrix}
7.18 & 6.43 & 6.56 & 5.78 & 6.85 & 5.58 & 6.46 & 4.97 & 6.79 & 5.90 & 5.30 & 5.99 & 6.18 & 6.23 & 5.76 & 6.76 & 5.61 & 5.82 & 6.39 & 5.99\\
3.26 & 3.28 & 3.11 & 2.39 & 2.80 & 2.83 & 3.33 & 2.45 & 2.92 & 2.71 & 2.00 & 3.01 & 2.24 & 2.91 & 2.95 & 3.14 & 3.02 & 2.74 & 2.25 & 2.54\\
4.75 & 4.58 & 4.91 & 4.01 & 4.63 & 4.55 & 4.77 & 3.31 & 4.68 & 3.94 & 3.58 & 4.24 & 4.09 & 4.71 & 3.61 & 4.45 & 4.51 & 4.10 & 4.55 & 3.91\\
1.49 & 1.54 & 1.55 & 1.36 & 1.52 & 1.32 & 1.67 & 1.02 & 1.35 & 1.41 & 1.08 & 1.53 & 1.02 & 1.49 & 1.39 & 1.44 & 1.52 & 1.09 & 1.53 & 1.18
\end{pmatrix}$$

C:
$$\begin{pmatrix}
5.28 & 5.03 & 4.96 & 4.98 & 5.25 & 5.68 & 4.86 & 5.37 & 4.69 & 5.30 & 5.70 & 5.19 & 5.08 & 4.63 & 5.36 & 5.56 & 5.41 & 5.42 & 5.99 & 5.49\\
3.86 & 3.38 & 3.51 & 3.49 & 3.80 & 4.03 & 3.63 & 3.65 & 3.22 & 3.51 & 3.70 & 3.61 & 3.34 & 3.21 & 4.45 & 4.64 & 4.22 & 3.74 & 4.15 & 4.04\\
1.55 & 1.58 & 1.51 & 1.71 & 1.63 & 1.85 & 1.57 & 1.51 & 1.78 & 1.64 & 1.78 & 1.74 & 1.69 & 1.21 & 1.41 & 1.65 & 1.51 & 1.50 & 1.95 & 1.61\\
0.39 & 0.24 & 0.35 & 0.46 & 0.32 & 0.52 & 0.47 & 0.32 & 0.35 & 0.21 & 0.48 & 0.33 & 0.22 & 0.29 & 0.39 & 0.54 & 0.52 & 0.49 & 0.33 & 0.48
\end{pmatrix}$$

$$\text{D:}\begin{pmatrix} 7.38 & 6.73 & 6.76 & 6.08 & 7.05 & 5.88 & 6.66 & 5.27 & 6.99 & 6.20 & 5.50 & 6.29 & 6.38 & 6.53 & 5.96 & 7.06 & 5.81 & 6.12 & 6.59 & 6.29 \\ 3.56 & 3.48 & 3.41 & 2.59 & 3.10 & 3.03 & 3.63 & 2.65 & 3.22 & 2.91 & 2.30 & 3.21 & 2.54 & 3.11 & 3.25 & 3.34 & 3.32 & 2.94 & 2.55 & 2.74 \\ 4.95 & 4.68 & 5.11 & 4.11 & 4.83 & 4.65 & 4.97 & 3.41 & 4.88 & 4.04 & 3.78 & 4.34 & 4.29 & 4.81 & 3.81 & 4.55 & 4.71 & 4.20 & 4.75 & 4.01 \\ 1.59 & 1.64 & 1.65 & 1.46 & 1.62 & 1.42 & 1.77 & 1.12 & 1.45 & 1.51 & 1.18 & 1.63 & 1.12 & 1.59 & 1.49 & 1.54 & 1.62 & 1.19 & 1.63 & 1.28 \end{pmatrix}$$

For A, B, C, D, we get the mean value and the standard deviation of each characteristic, respectively. The mean value of A is $o_i = [4.9945;3.5215;1.4810;0.2375]$. And the standard deviation of A is $\delta_i = [0.3376;0.3884;0.1526;0.0551]$, $(i = 1,2,3,4)$. We will make the construction of trapezoidal fuzzy numbers. Let $u = (u_1, u_2, u_3, u_4)$.

$$u_i(x_i) = \begin{cases} \dfrac{x_i - (o_i - \beta_1\delta_i)}{(\beta_1 - \beta_2)\delta_i} & x_i \in [o_i - \beta_1\delta_i, o_i - \beta_2\delta_i] \\ 1 & x_i \in [o_i - \beta_2\delta_i, o_i + \beta_3\delta_i] \\ \dfrac{x_i - (o_i + \beta_4\delta_i)}{(\beta_3 - \beta_4)\delta_i} & x_i \in [o_i + \beta_3\delta_i, o_i + \beta_4\delta_i] \\ 0, & \text{else} \end{cases}, \quad i = 1,2,3,4$$

Then $u_i = (o_i - \beta_1\delta_i, o_i - \beta_2\delta_i,\ o_i + \beta_3\delta_i,\ o_i + \beta_4\delta_i)^{\mathrm{T}}$, $\beta_i \geq 0$ are parameters. So, we get $n-$ frustum pyramid fuzzy number u which represents flower A. In the same way, we can get $n-$ frustum pyramid fuzzy number v, w, q represent flower B, C, D, respectively. Let $\beta_1 = \beta_4 = 3, \beta_2 = \beta_3 = 1$, we have

$$u = \begin{pmatrix} 3.9817 & 2.3562 & 1.0232 & 0.0721 \\ 4.6596 & 3.1331 & 1.3248 & 0.1824 \\ 5.3321 & 3.9099 & 1.6336 & 0.2926 \\ 6.0073 & 4.6868 & 1.9388 & 0.4029 \end{pmatrix}, v = \begin{pmatrix} 4.4446 & 1.6626 & 2.9323 & 0.7872 \\ 5.5659 & 2.4169 & 3.8401 & 1.1791 \\ 6.6871 & 3.1711 & 4.7479 & 1.5709 \\ 7.8084 & 3.9254 & 5.6557 & 1.9628 \end{pmatrix}$$

$$w = \begin{pmatrix} 4.2272 & 2.5778 & 1.1257 & 0.0716 \\ 4.9167 & 3.3653 & 1.4546 & 0.2805 \\ 5.6063 & 4.1527 & 1.7834 & 0.4895 \\ 6.2958 & 4.9402 & 2.1123 & 0.6884 \end{pmatrix}, q = \begin{pmatrix} 4.7392 & 1.9047 & 3.0348 & 0.8872 \\ 5.8307 & 2.6642 & 3.9743 & 1.2791 \\ 6.9223 & 3.4238 & 4.9137 & 1.6709 \\ 8.0138 & 4.1833 & 5.8532 & 2.0628 \end{pmatrix}$$

Let $\alpha = (0.25,0.25,0.25,0.25)$, and $p = 0.9$. We have

$$G_{\alpha,p}(u,v) = 0.5437; G_{\alpha,p}(u,w) = 0.8669; G_{\alpha,p}(u,q) = 0.5033;$$
$$G_{\alpha,p}(v,w) = 0.5931; G_{\alpha,p}(v,q) = 0.8710; G_{\alpha,p}(w,q) = 0.5455.$$

Obviously, we can put A, C in a group and B, C in another group.

Acknowledgments. This work is supported by Natural Science Foundation of China (No.60934009).

References

1. Zadeh, L.A.: Fuzzy Sets. Information Control, 338–353 (1965)
2. Chang, S.S.L., Zadeh, L.A.: On fuzzy mappings and control. IEEE Trans. Syst. Man Cybernet. 2, 30–34 (1972)
3. Wang, G.X., Wu, C.X.: Fuzzy n-cell Numbers and the Differential of Fuzzy n-cell Value Mappings. Fuzzy Sets and System 130, 367–381 (2003)
4. Wang, G.X., Li, Y.M., Wen, C.L.: On Fuzzy n-cell Numbers and n-dimension Fuzzy Vectors. Fuzzy Sets and system 158, 71–84 (2007)
5. Wang, G.X., Shi, P., Messenger, P.: Representation of uncertain Multi-Channel Digital Signal Spaces and Study of Pattern Recognition Based on Metrics and Difference Values on Fuzzy n-cell Number Spaces. IEEE Trans. on Fuzzy systems 17(2), 421–439 (2009)
6. Wang, G.X., Shi, P., Wen, C.L.: Fuzzy approximation relations on fuzzy n-cell number space and their applications in classification. Information Sciences 181, 3846–3860 (2011)

Similarity Relation of Two-Dimensional Frustum Pyramid Fuzzy Numbers Based on the Geometry and Its Application

Jie Du, Guixiang Wang, and Jiaxi Zhang

Institute of Operational Research and Cybernetics,
Hangzhou Dianzi University, Hangzhou, 310018, China
dujie_41@163.com

Abstract. In this article, we define a similarity relation of two-dimensional frustum pyramid fuzzy numbers, and discuss its properties, and use the similarity relation to rank some uncertain attributes (e.g. the observing of Eigen values of target is uncertain or imprecise observation). The similarity relation is given out according to the definition of the virtual center of gravity and volume of two-dimensional frustum pyramid fuzzy numbers. In this article, we give an example to illustrate the similarity relation is reasonable in the actual application.

Keywords: Virtual center of gravity, volume, similarity relation of fuzzy numbers, ranking.

1 Introduction

In recent years, many scholars have studied on the similarity relation of fuzzy numbers. Lee [1], Hsieh-and-Chen [2], Chen-and-Chen [3], and Chen-and-Lin [4], discuss in the similarity relation, but these methods have some shortcomings. Then, based on the traditional center of gravity method, Chen improved the past insufficient. But in the life, there're many targets with some uncertain attributes can't be solved by the one-dimensional trapezoidal fuzzy numbers because they have multidimensional attributes. Therefore, seeking a method for similarity relation of multidimensional fuzzy numbers is a useful job. This article mainly gives the definition of similarity relation of two-dimensional frustum pyramid fuzzy numbers, discusses its properties, and ranks the targets with some uncertain attributes by the similarity relation. This method combines geometry distance with the virtual center of gravity and volume of two-dimensional frustum pyramid fuzzy numbers together to depict the similarity relation of two-dimensional frustum pyramid fuzzy numbers. The method has some characteristics, such as simple calculation, convenient application, and the results obtained are more rationality, and so on.

D. Yang (Ed.): Informatics in Control, Automation and Robotics, Volume 2, LNEE 133, pp. 49–57.
springerlink.com

2 Preliminaries

In the literature [5], [6], the fuzzy numbers that author discussed is regular, i.e. the maximum value of membership function is 1. In order to apply more widely, the fuzzy numbers this paper relates to does not necessarily require that they are normal, the value of membership function is not 1 can be allowed, i.e. the fuzzy numbers whose maximum value of membership function is ω $(0<\omega\le 1)$.

2.1 Trapezoidal Fuzzy Numbers

Denote the R as the set of real numbers, $F(R)$ as all the fuzzy subset of R, i.e. $F(R)=\{u \mid u: R\to[0,1]\}$. $u\in F(R)$, $a,b,c,d\in R$ and $a\le b\le c\le d$, $\omega\in(0,1]$. If the membership function of u satisfies

$$u(x)=\begin{cases}\dfrac{\omega(x-a)}{b-a}, & a\le x<b\\ \omega, & b\le x<c\\ \dfrac{\omega(x-d)}{c-d}, & c\le x<d\\ 0, & x\notin[a,d]\end{cases},$$

then u is called trapezoid fuzzy numbers, denotes as $u=(a,b,c,d;\omega)$.

2.2 Two-Dimensional Frustum Pyramid Fuzzy Numbers

Definition 1: Assume $a_i,b_i,c_i,d_i\in R$ and $a_i\le b_i\le c_i\le d_i$, $\omega\in(0,1]$. $u\in F(R^2)$ $F(R^2)=\{u \mid u: R^2\to[0,1]\}$, which R^2 is the Cartesian product of R and R. If u satisfies: when $(x_1,x_2)\notin[a_1,d_1]\times[a_2,d_2]$, then $u(x_1,x_2)=0$; when $(x_1,x_2)\in[a_1,d_1]\times[a_2,d_2]$, then the value of $u(x_1,x_2)$ is formed by the side and up bottom of 4 pyramid whose up bottom and down bottom are respectively composed by $\{(x_1,x_2,x_3):(x_1,x_2)\in[b_1,c_1]\times[b_2,c_2],x_3=\omega\}$ and $\{(x_1,x_2,x_3):(x_1,x_2)\in[a_1,d_1]\times[a_2,d_2],x_3=0\}$, i.e. the point $(x_1,x_2,u(x_1,x_2))$ is on the side and up bottom of 4 pyramid, then the u is called two-dimensional frustum pyramid fuzzy numbers, denotes as $\begin{bmatrix}a_1 & b_1 & c_1 & d_1 & \omega\\ a_2 & b_2 & c_2 & d_2\end{bmatrix}$. Assume $a_i,b_i,c_i,d_i\in R$ and $a_i\le b_i\le c_i\le d_i$, $\omega_i\in(0,1]$. $u_i=(a_i,b_i,c_i,d_i;\omega_i)$, $(i=1,2)$ are trapezoidal fuzzy numbers, then $u=\begin{bmatrix}a_1 & b_1 & c_1 & d_1 & \omega\\ a_2 & b_2 & c_2 & d_2\end{bmatrix}$ is called two-dimensional frustum pyramid fuzzy numbers which is induced by u_1 and u_2, denotes as $u=[u_1,u_2]^T$ or $u=\begin{bmatrix}a_1 & b_1 & c_1 & d_1 & \omega_1\\ a_2 & b_2 & c_2 & d_2 & \omega_2\end{bmatrix}$, i.e. $\begin{bmatrix}a_1 & b_1 & c_1 & d_1 & \omega_1\\ a_2 & b_2 & c_2 & d_2 & \omega_2\end{bmatrix}=\begin{bmatrix}a_1 & b_1 & c_1 & d_1 & \omega\\ a_2 & b_2 & c_2 & d_2\end{bmatrix}$, in which $\omega=\min(\omega_1,\omega_2)$. The Fig.1 is shown as follows.

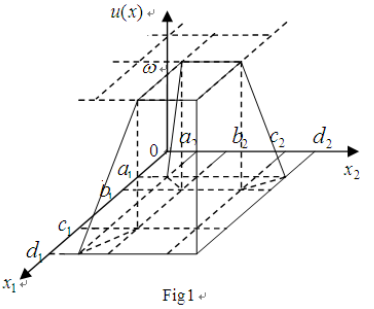

Fig 1

2.3 Several Special Two-Dimensional Frustum Pyramid Fuzzy Numbers

Assume $u=\begin{bmatrix} a_1 & b_1 & c_1 & d_1 & \omega \\ a_2 & b_2 & c_2 & d_2 & \end{bmatrix}$ is a two-dimensional frustum pyramid fuzzy numbers, in which $a_i,b_i,c_i,d_i \in R$ and $a_i \le b_i \le c_i \le d_i$, $\omega \in (0,1]$. Then

i) If $\omega=1$, then u is called a normal two-dimensional frustum pyramid fuzzy numbers;

ii) If $a_1=a_2,b_1=b_2,c_1=c_2,d_1=d_2$, then u is called a isosceles two-dimensional frustum pyramid fuzzy numbers;

iii) If $b_1=c_1,b_2=c_2$, then u is called a pyramidal fuzzy numbers;

iv) If $a_1=b_1,c_1=d_1,a_2=b_2,c_2=d_2$, then u is called a prismatic fuzzy numbers;

v) If $a_1=b_1=c_1=d_1,a_2=b_2=c_2=d_2$, then u is called a fuzzy point.

2.4 The Fuzzy Operations between Two-Dimensional Frustum Pyramid Fuzzy Numbers

In the literature [7], the author has given out the operations between trapezoidal fuzzy numbers. It is shown as follows:

Assume $u=(a_u,b_u,c_u,d_u;\omega_u)$ and $v=(a_v,b_v,c_v,d_v;\omega_v)$ are two trapezoidal fuzzy numbers, and k is a constant, then

a) $u+v=(a_u+a_v,b_u+b_v,c_u+c_v,d_u+d_v;\min\{\omega_u,\omega_v\})$;

b) $ku=(ka_u,kb_u,kc_u,kd_u;\omega_u)$;

c) $u\cdot v=(a_u\times a_v,b_u\times b_v,c_u\times c_v,d_u\times d_v;\min\{\omega_u,\omega_v\})$.

Then we give out the definition of fuzzy operations between two-dimensional frustum pyramid fuzzy numbers:

Definition 2: Assume $u=\begin{bmatrix} a_{u1} & b_{u1} & c_{u1} & d_{u1} & \omega_u \\ a_{u2} & b_{u2} & c_{u2} & d_{u2} & \end{bmatrix}, v=\begin{bmatrix} a_{v1} & b_{v1} & c_{v1} & d_{v1} & \omega_v \\ a_{v2} & b_{v2} & c_{v2} & d_{v2} & \end{bmatrix}$ are two-dimensional frustum pyramid fuzzy numbers, and k is a constant, then the fuzzy operations are shown as follows:

$$1)\ u+v=\begin{bmatrix} a_{u1}+a_{v1} & b_{u1}+b_{v1} & c_{u1}+c_{v1} & d_{u1}+d_{v1} & \min\{\omega_u,\omega_v\} \\ a_{u2}+a_{v2} & b_{u2}+b_{v2} & c_{u2}+c_{v2} & d_{u2}+d_{v2} & \end{bmatrix};$$

$$2)\ ku=\begin{bmatrix} ka_{u1} & kb_{u1} & kc_{u1} & kd_{u1} & \omega_u \\ ka_{u2} & kb_{u2} & kc_{u2} & kd_{u2} & \end{bmatrix};$$

$$3)\ u\cdot v=\begin{bmatrix} a_{u1}\times a_{v1} & b_{u1}\times b_{v1} & c_{u1}\times c_{v1} & d_{u1}\times d_{v1} & \min\{\omega_u,\omega_v\} \\ a_{u2}\times a_{v2} & b_{u2}\times b_{v2} & c_{u2}\times c_{v2} & d_{u2}\times d_{v2} & \end{bmatrix}.$$

***Proposition 1**:* Assume u_1,u_2,v_1,v_2 are trapezoidal fuzzy numbers, $u=[u_1,u_2]^T$, and $v=[v_1,v_2]^T$ are two-dimensional frustum pyramid fuzzy numbers which are induced by u_1,u_2 and v_1,v_2 respectively, and k is a constant. Then

1) $u+v=[u_1+v_1,u_2+v_2]^T$;

2) $ku=[ku_1,ku_2]^T$;

3) $u\cdot v=[u_1\cdot v_1,u_2\cdot v_2]^T$.

Proof: Assume $u_i=(a_{ui},b_{ui},c_{ui},d_{ui};\omega_{ui})$ and $v_i=(a_{vi},b_{vi},c_{vi},d_{vi};\omega_{vi})\ (i=1,2)$.

1) On one hand, according to the definition of two-dimensional frustum pyramid fuzzy numbers which is induced by two trapezoidal fuzzy numbers, we can see that

$$u=[u_1,u_2]^T=\begin{bmatrix} a_{u1} & b_{u1} & c_{u1} & d_{u1} & \omega_{u1} \\ a_{u2} & b_{u2} & c_{u2} & d_{u2} & \omega_{u2} \end{bmatrix}=\begin{bmatrix} a_{u1} & b_{u1} & c_{u1} & d_{u1} & \min\{\omega_{u1},\omega_{u2}\} \\ a_{u2} & b_{u2} & c_{u2} & d_{u2} & \end{bmatrix},$$

$$v=[v_1,v_2]^T=\begin{bmatrix} a_{v1} & b_{v1} & c_{v1} & d_{v1} & \omega_{v1} \\ a_{v2} & b_{v2} & c_{v2} & d_{v2} & \omega_{v2} \end{bmatrix}=\begin{bmatrix} a_{v1} & b_{v1} & c_{v1} & d_{v1} & \min\{\omega_{v1},\omega_{v2}\} \\ a_{v2} & b_{v2} & c_{v2} & d_{v2} & \end{bmatrix}.$$

Also according to the definition of two-dimensional frustum pyramid fuzzy numbers addition, we can see that

$$u+v=\begin{bmatrix} a_{u1}+a_{v1} & b_{u1}+b_{v1} & c_{u1}+c_{v1} & d_{u1}+d_{v1} & \min\{\omega_{u1},\omega_{u2},\omega_{v1},\omega_{v2}\} \\ a_{u2}+a_{v2} & b_{u2}+b_{v2} & c_{u2}+c_{v2} & d_{u2}+d_{v2} & \end{bmatrix}.$$

On the other hand, according to the definition of the trapezoidal fuzzy numbers addition and the definition of two-dimensional frustum pyramid fuzzy numbers which is induced by two trapezoidal fuzzy numbers, we can see that

$$[u_1+v_1,u_2+v_2]^T=\begin{bmatrix} a_{u1}+a_{v1} & b_{u1}+b_{v1} & c_{u1}+c_{v1} & d_{u1}+d_{v1} & \min\{\omega_{u1},\omega_{v1}\} \\ a_{u2}+a_{v2} & b_{u2}+b_{v2} & c_{u2}+c_{v2} & d_{u2}+d_{v2} & \min\{\omega_{u2},\omega_{v2}\} \end{bmatrix}$$
$$=\begin{bmatrix} a_{u1}+a_{v1} & b_{u1}+b_{v1} & c_{u1}+c_{v1} & d_{u1}+d_{v1} & \min\{\omega_{u1},\omega_{v1},\omega_{u2},\omega_{v2}\} \\ a_{u2}+a_{v2} & b_{u2}+b_{v2} & c_{u2}+c_{v2} & d_{u2}+d_{v2} & \end{bmatrix}.$$

Therefore, $u+v=[u_1+v_1,u_2+v_2]^T$ is established.

2) On one hand, according to the definition of two-dimensional frustum pyramid fuzzy numbers which is induced by two trapezoidal fuzzy numbers, we can see that

$$u=[u_1,u_2]^T=\begin{bmatrix} a_{u1} & b_{u1} & c_{u1} & d_{u1} & \omega_{u1} \\ a_{u2} & b_{u2} & c_{u2} & d_{u2} & \omega_{u2} \end{bmatrix}=\begin{bmatrix} a_{u1} & b_{u1} & c_{u1} & d_{u1} & \\ a_{u2} & b_{u2} & c_{u2} & d_{u2} & \min\{\omega_{u1},\omega_{u2}\} \end{bmatrix},$$

Also according to the definition of two-dimensional frustum pyramid fuzzy numbers scalar multiplication, we can see that

$$ku=\begin{bmatrix} a_{u1} & b_{u1} & c_{u1} & d_{u1} & \\ a_{u2} & b_{u2} & c_{u2} & d_{u2} & \min\{\omega_{u1},\omega_{u2}\} \end{bmatrix}.$$

On the other hand, according to the definition of the trapezoidal fuzzy numbers scalar multiplication and the definition of two-dimensional frustum pyramid fuzzy numbers which is induced by two trapezoidal fuzzy numbers, we can see that

$$[ku_1,ku_2]^T=\begin{bmatrix} ka_{u1} & kb_{u1} & kc_{u1} & kd_{u1} & \omega_{u1} \\ ka_{u2} & kb_{u2} & kc_{u2} & kd_{u2} & \omega_{u2} \end{bmatrix}=\begin{bmatrix} ka_{u1} & kb_{u1} & kc_{u1} & kd_{u1} & \\ ka_{u2} & kb_{u2} & kc_{u2} & kd_{u2} & \min\{\omega_{u1},\omega_{u2}\} \end{bmatrix}.$$

Therefore, $ku=[ku_1,ku_2]^T$ is established.

3) The proof method is similar with the two former methods.

3 Geometrical Quantity of Two-Dimensional Frustum Pyramid Fuzzy Numbers

We know that calculating the center of gravity of a three-dimensional graphics is used the method of triple integral. The method is shown as follows: Let V be an object in space whose density function is $\rho(x,y,z)$, and $\rho(x,y,z)$ is continuous in the V. When the density of the object V is uniform, i.e. $\rho(x,y,z)$ is a constant, then the center of gravity coordinate of the space object is

$$\bar{x}=\frac{1}{V}\iiint xdV \qquad \bar{y}=\frac{1}{V}\iiint ydV \qquad \bar{z}=\frac{1}{V}\iiint zdV \tag{1}$$

Then the points which two-dimensional frustum pyramid fuzzy numbers corresponds to are on the side and up bottom of 4 pyramid, and the graphics which is composed by two-dimensional frustum pyramid fuzzy numbers can be seen as an object with uniform density in space. Therefore, according to (1), we can get the center of gravity of two-dimensional frustum pyramid fuzzy numbers. It is complex to compute the center of gravity of two-dimensional frustum pyramid fuzzy numbers with the method of triple integral and the amount of calculation is large. And this method can not calculate the center of gravity of fuzzy point. So we put forward to a new method to calculate the center of gravity of two-dimensional frustum pyramid fuzzy numbers.

Assume $u=\begin{bmatrix} a_1 & b_1 & c_1 & d_1 & \\ a_2 & b_2 & c_2 & d_2 & \omega \end{bmatrix}$ is a two-dimensional frustum pyramid fuzzy numbers, $a_i,b_i,c_i,d_i\in R$ and $a_i\le b_i\le c_i\le d_i, i=1,2.\omega\in(0,1]$. Then the definition of virtual center of gravity is shown as follows:

$$y=\begin{cases}\dfrac{\omega\left(\dfrac{(c_1-b_1)(c_2-b_2)}{(d_1-a_1)(d_2-a_2)}+2\right)}{6}, & d_1\neq a_1, d_2\neq a_2,\\ \dfrac{\omega}{2}, & \text{others}\end{cases}$$

$$\begin{cases}x_1=\dfrac{c_2+b_2-(d_2+a_2)}{2\omega}y+\dfrac{d_2+a_2}{2}\\ x_2=\dfrac{c_1+b_1-(d_1+a_1)}{2\omega}y+\dfrac{d_1+a_1}{2}\end{cases}, d_1\neq a_1, d_2\neq a_2, \begin{cases}x_1=\dfrac{d_2+a_2}{2}\\ x_2=\dfrac{d_1+a_1}{2}\end{cases}, \text{others}. \quad (2)$$

The definition of volume is shown as follows:

$$V=\begin{cases}\dfrac{\omega}{2}\left[(d_1-a_1)+(c_1-b_1)+(d_2-a_2)+(c_2-b_2)\right] & a_1=d_1 \text{ or } a_2=d_2\\ \dfrac{\omega}{2}\left[(d_1-a_1)(d_2-a_2)+3(c_1-b_1)(c_2-b_2)\right] & \text{others}\end{cases} \quad (3)$$

4 Similarity Relation between Two-Dimensional Frustum Pyramid Fuzzy Numbers

In discussing the problem of ranking two-dimensional frustum pyramid fuzzy numbers whose two component are both trapezoidal fuzzy numbers, in order to unify dimension, we restrict that the parameters a,b,c,d satisfies $0\le a\le b\le c\le d\le 1$.

Definition 3: Assume $u=\begin{bmatrix}a_1 & b_1 & c_1 & d_1 & \omega\\ a_2 & b_2 & c_2 & d_2 & \end{bmatrix}$ and $v=\begin{bmatrix}a_1' & b_1' & c_1' & d_1' & \omega'\\ a_2' & b_2' & c_2' & d_2' & \end{bmatrix}$ are two two-dimensional frustum pyramid fuzzy numbers, in which $0\le a_i\le b_i\le c_i\le d_i\le 1$, $0\le a_i'\le b_i'\le c_i'\le d_i'\le 1, i=1,2$, and $\omega,\omega'\in(0,1]$. Then the similarity between u and v is shown as follows:

$$S(u,v)=\left(1-\frac{\sum_{i=1}^{2}\left(\left|a_i-a_i'\right|+\left|b_i-b_i'\right|+\left|c_i-c_i'\right|+\left|d_i-d_i'\right|\right)}{2\sum_{i=1}^{2}\dfrac{\left|d_i+d_i'\right|}{B(a_i,a_i')}+C(a_i,a_i')}\right)\times\frac{1}{1+\left|x_1-x_1'\right|+\left|x_2-x_2'\right|}\times\left[1-(V_u-V_v)\right]\times\frac{\min\{\omega,\omega'\}}{\max\{\omega,\omega'\}},$$

in which $B(a_i,a_i')=\begin{cases}1, & a_i=0,a_i'=0\\ \left|a_i+a_i'\right|, & \text{others}\end{cases}$, $C(a_i,a_i')=\begin{cases}4, & a_i=0,a_i'=0\\ 0, & \text{others}\end{cases}$.

4.1 The Properties of Similarity Relation

Property 1: Two-dimensional frustum pyramid fuzzy numbers u, v are identical if and only if $S(u,v)=1$.

Proof: ($\Rightarrow$) If u and v are identical, we can see that $a_i = a_i^{'}, b_i = b_i^{'}, c_i = c_i^{'}$, $d_i = d_i^{'}$, and . Thus, according to (2), (3) we can get the virtual center of gravity and the value of volume. We can see that $x_1 = x_1^{'}, x_2 = x_2^{'}, V_u = V_v$. If $a_i = 0, a_i^{'} = 0$, then $B(a_i, a_i^{'}) = 1$, So $S(u,v) = 1$. If a_i and $a_i^{'}$ are others, then $B(a_i, a_i^{'}) = \left| a_i + a_i^{'} \right|$, $C(a_i, a_i^{'}) = 0$. So $S(u,v) = 1$. Therefore we can see that $S(u,v) = 1$.

($\Leftarrow$) If $S(u,v) = 1$, then $\sum_{i=1}^{2} \left(\left| a_i - a_i^{'} \right| + \left| b_i - b_i^{'} \right| + \left| c_i - c_i^{'} \right| + \left| d_i - d_i^{'} \right| \right) = 0$, it implies that $a_i = a_i^{'}, b_i = b_i^{'}, c_i = c_i^{'}, d_i = d_i^{'}, i = 1,2$. According to the definition of similarity relation, we can see that $\frac{\min\left\{\omega, \omega^{'}\right\}}{\max\left\{\omega, \omega^{'}\right\}} = 1$, so $\omega = \omega^{'}$. From (2) and (3), we can see that $x_1 = x_1^{'}$, $x_2 = x_2^{'}, V_u = V_v$. Therefore, we can get $u = v$.

Property 2: $S(u,v) = S(v,u)$.

Proof: According to the definition of similarity relation of two-dimensional frustum pyramid fuzzy numbers, we can see that it is right obviously.

Property 3: If $u = \begin{bmatrix} a & a & a & a & 1 \\ b & b & b & b & \end{bmatrix}$ and $v = \begin{bmatrix} a^{'} & a^{'} & a^{'} & a^{'} & 1 \\ b^{'} & b^{'} & b^{'} & b^{'} & \end{bmatrix}$ are two-dimensional frustum pyramid fuzzy numbers. Then $S(u,v) = 1 - \left| a - a^{'} \right| - \left| b - b^{'} \right|$.

Proof: From (2) and (3), we can see that $x_1 = x_1^{'}, x_2 = x_2^{'}, V_u = V_v$. If $a_i = 0, a_i^{'} = 0$, $a_i^{'} = 0$, then $B(a_i, a_i^{'}) = 1, C(a_i, a_i^{'}) = 4$. Thus $S(u,v) = 1 - \left| a - a^{'} \right| - \left| b - b^{'} \right|$. If a_i and $a_i^{'}$ are other values, then $B(a_i, a_i^{'}) = \left| a_i + a_i^{'} \right|, C(a_i, a_i^{'}) = 0$, thus $S(u,v) = 1 - \left| a - a^{'} \right| - \left| b - b^{'} \right|$.

Assume $u = (u_1, u_2)$ and $v = (v_1, v_2)$ are two-dimensional fuzzy vectors, u_1, u_2 and v_1, v_2 are both trapezoid fuzzy numbers, then the similarity between u and v is defined as the similarity between the two-dimensional frustum pyramid fuzzy numbers which are induced respectively by u_1, u_2 and v_1, v_2 , and denotes as $S(u,v)$, too.

5 The Example for Practical Application

Example: To a producer, the good or bad working state of the producer is related to the product quantity and quality in one working day. The following data is obtained from a factory with 10 producers' work performance in 10 days.

	P_{11}	P_{21}	P_{31}	P_{41}	P_{51}	P_{61}	P_{71}	P_{81}	P_{91}	P_{101}	P_{12}	P_{22}	P_{32}	P_{42}	P_{52}	P_{62}	P_{72}	P_{82}	P_{92}	P_{102}
D_1	1200	1173	1107	994	1092	1092	1153	1200	1051	1093	98.3	98.4	94.3	87.8	89.4	89.3	93.7	96.3	98.4	95.6
D_2	1000	1042	1128	1200	1038	1086	1129	1198	1033	1120	99.2	97.1	97.5	89.9	94.5	94.5	91.4	98.6	94.6	97.1
D_3	1101	997	928	1036	1259	1102	1084	1145	998	1139	9801	97.9	89.9	92.6	93.4	88.8	91.8	99.1	95.4	98.3
D_4	980	935	1148	1029	994	1117	1078	1138	1173	1140	98.9	99.4	90.3	90.6	96.6	93.5	89.9	98.3	97.5	95.3
D_5	993	1102	974	1147	1100	1185	992	983	1039	1203	94.8	98.1	91.5	89.7	96.3	93.8	97.7	91.3	96.1	96.2
D_6	968	1098	1250	1083	1048	950	994	995	1167	1240	99.3	98.0	96.7	86.8	97.6	84.9	98.9	91.2	94.6	94.8
D_7	1150	1163	985	981	1176	1130	1041	998	1193	993	98.1	96.9	88.7	90.5	95.4	89.5	96.4	93.3	96.8	93.5
D_8	1012	1058	990	937	1093	989	1021	1001	1129	989	98.5	97.1	92.9	93.4	97.1	92.7	96.5	94.9	99.5	96.4
D_9	1121	954	1046	1102	1094	994	1232	1038	1102	993	99.1	98.5	94.2	91.8	98.8	94.4	95.3	94.7	95.4	97.2
D_{10}	1034	1203	1092	1096	1101	1019	1192	1129	1029	1067	98.7	99.3	94.6	93.8	94.4	91.5	94.9	97.5	96.4	95.9

We denote P_{i1} where $P_{i1} \in [0,+\infty], i = 1,2$, as the number of products what the first i person (denotes as P_i) produce (unit: part) in one day. And we denote P_{i2} where $P_{i2} \in [0,100]$, $i = 1,2,\cdots 10$ as the production of the qualified rate of products what the first i individual produce (unit :%) in one day. Denote D_i as the first i day. We need to sort the 10 producers.

For each of their "ten day's working state", we can construct a two-dimensional fuzzy vectors $u_{P_i} = \left(u_{P_i}^j, u_{P_i}^j\right), i = 1,2,\cdots 10, j = 1,2$. According to (2) and (3), we can obtain respectively the volumes and virtual centers of gravity of ten two-dimensional frustum pyramid fuzzy numbers. To everyday, take the maximum value of the number of products and the highest qualified rate of products what the 10 individuals product, and then we can construct an "ideal state standard" P'. To P', we can also construct a two-dimensional fuzzy vector $u_{P'} = \left(u_P^1, u_P^2\right)$. According to the definition of similarity relation between two-dimensional frustum pyramid fuzzy numbers, we can obtain the similarity between $u_{P'}$ and $u_{P_i}\left(i = 1,2,\cdots 10\right)$,i.e. $S(u_{P_3}, u_{P'}) = 0.5502$, $S(u_{P_4}, u_{P'}) = 0.5479$, $S(u_{P_5}, u_{P'}) = 0.5152$, $S(u_{P_6}, u_{P'}) = 0.5886$, $S(u_{P_7}, u_{P'}) = 0.6274$, $S(u_{P_8}, u_{P'}) = 0.6019$, $S(u_{P_9}, u_{P'}) = 0.7057$, $S(u_{P_{10}}, u_{P'}) = 0.5695$. Then in order to know which producer is better performance, we can make a comparison between the "ten day's working state" of ten produces and the "ideal state standard". Obviously, $S(u_{P_1}, u_{P'}) = 0.7233$ is the biggest. Therefore, we can believe the producer P_1 is better performance than others.

Acknowledgments. This work is supported by Natural Science Foundations of China (No. 60934009).

References

1. Lee, H.S.: An Optimal Aggregation Method for Fuzzy Opinions of Group Decision. In: Proc. 1999 IEEE Int. Conf. Systems, Man, Cybernetics, vol. 3, pp. 314–319 (1999)
2. Hsieh, C.H., Chen, S.H.: Similarity of Generalized Fuzzy Numbers with Graded Mean Integration Representation. In: Proc. 8th Int. Fuzzy Systems Association World Congr., Taipei, Taiwan, Republic of China, vol. 2, pp. 551–555 (1999)

3. Chen, S.J., Chen, S.M.: A New Simple Center-of-gravity Method for Handling the Fuzzy Ranking and the Defuzzification Problems. In: 8th National Conf. Fuzzy Theory Applications, Taipei, Taiwan, Republic of China (2000)
4. Chen, S.M.: New Methods for Subjective Mental Workload Assessment and Fuzzy Risk Analysis. Cybern. Syst.: Int. J. 27(5), 449–472 (1996)
5. Wang, G.X., Wu, C.X.: Fuzzy n-cell Numbers and the Differential of Fuzzy n-cell Value Mappings. Fuzzy Sets and System 130, 367–381 (2003)
6. Wang, G.X., Li, Y.M., Wen, C.L.: On Fuzzy n-cell Numbers and n-dimension Fuzzy Vectors. Fuzzy Sets and System 158, 71–84 (2007)
7. Chen, S.J.: Fuzzy Risk Analysis Based on Similarity Measures of Generalized Fuzzy Numbers. IEEE Transactions on Fuzzy Systems 11, 45–56 (2003)

Robust Controller Design for One Arm Space Manipulator with Uncertainties Compensated

Guangyan Xu, Meng Zhang, and Huanqiang Wang

School of Automation, Shenyang Aerospace University
110136, Shenyang, China
Guangyan_xu@163.com

Abstract. According to trajectory tracking control of space robot with parameters uncertainties, the disturbance on space robot trajectory tracking is taken into consideration. Firstly, robust controller is applied to compensate the coriolis force, centrifugal force and other disturbance. Robust control law with items uncertainties compensated is improved. The desired time-varying trajectory can be real-time tracked by manipulators while the attitude of space robot can be controlled. The compensation matrix is proposed. Uncertainty item range can be solved based on PSO and it can be applied to control manipulators. The simulation results show that the robust controller has a good performance.

Keywords: space manipulator, trajectory tracking, robust control, disturbance compensated.

1 Introduction

Free flying space robot will be widely applied to accomplish space tasks. Trajectory tracking is not only helpful to complete space missions but also reduce the disturbance to attitude. Therefore, the attitude can be controlled while space tasks are accomplished.

Many domestic and foreign experts have a thorough research in the fields of dynamics analysis, attitude control and trajectory tracking. An adaptive robust controller for one-arm space manipulator is designed to accomplish trajectory tracking and the stability analysis is based on Lyapunov theory[1]. RBF neutral network is applied to approach the nonlinear dynamics model of space robot, and then tracking control based on robust controller in space task is researched[2]. In paper[3], an adaptive controller is designed by GU YL. The results show that it has a good performance in trajectory tracking. However, dynamics equations are needed to be linearization and complex pre-calculation is needed to derive regression matrix. In fact, the regression matrix is difficult to obtain for the complex of space robot. The dynamics model of the space robot is derived based on Generalized Jacobin Matrix by Chen L and the corporative motion of joint and attitude is completed by the robust adaptive controller [4]. An optimization of minimum fuel consumption is derived by WF XU. Joint motion is planned to control the attitude and joint angles [5]. A.Green and J.Z.Sasiadek respectively apply inverse flexible dynamics control (IFDC) and fuzzy logic system adaptive control (FLSAC) to control the flexible space

D. Yang (Ed.): Informatics in Control, Automation and Robotics, Volume 2, LNEE 133, pp. 59–66.
springerlink.com

manipulators. Simulation results show that joint motion has a greatly disturbance to the orbits of space robot when IFDC is the control strategy. In contrast, FLSAC control strategy has a better performance[6]. However, there are too much computing. A robust adaptive controller is designed to control trajectory based on E.Platform[7]. In paper[8], on the base of PD control strategy, a decentralized nonlinear robust control is proposed. The tracking error is global convergence. In paper [9], the optimization of trajectory tracking can be derived by Karol when the space craft is docking. Experiments prove that the controller has a good effect, but the attitude of space manipulator is no taken into consideration.

In the paper, space robot with parameters uncertainties compensated is controlled based on robust control theory of uncertainty-system. Firstly, centrifugal, coriolis forces and attitude disturbance are compensated and the control law is improved to avoid the singular. Stability analysis is proved by Lyapunov theory. In order to solve the ranges of uncertainty-parameters and improve the performance, Practical Swarm Optimization is applied to obtain the compensated matrix. Global exponential stability of Robust controller is the difference.

Compared with paper[10], control law is improved and Robust controller is global exponential stability. Especially, control torque is more slightly. Simulation results show that it has a better performance than the previous controller.

2 Dynamics Equations of Space Robot

Dynamics equations of space robot with n rigid body are derived based on Lagrange Equations. Geopotential energy and Perturbing force are ignored. Dynamics equations of multi-rigid body space robot are given by:

$$M_{11}(\mathbf{q})\ddot{\boldsymbol{\varphi}} + M_{12}(\mathbf{q})\ddot{\boldsymbol{\theta}} + C_1(\mathbf{q},\dot{\mathbf{q}})\dot{\mathbf{q}} = G\boldsymbol{\tau}_{\varphi} \tag{1}$$

$$M_{21}(\mathbf{q})\ddot{\boldsymbol{\varphi}} + M_{22}(\mathbf{q})\ddot{\boldsymbol{\theta}} + C_2(\mathbf{q},\dot{\mathbf{q}})\dot{\mathbf{q}} = \boldsymbol{\tau}_{\theta} \tag{2}$$

$$C_2(\mathbf{q},\dot{\mathbf{q}}) = \sum_{j=1}^{3+n} \dot{q}_j C_{2j}(\mathbf{q}) \tag{3}$$

Where $\boldsymbol{\varphi} \in R^{3\times 1}$ is attitude vector, $\boldsymbol{\theta} \in R^{n\times 1}$ is the vector of space manipulator joint angles. n stands for the number of kinematic pairs, $\mathrm{q}=[\boldsymbol{\varphi}^T \quad \boldsymbol{\theta}^T]^T \in R^{3+n}$ is the vector of generalized coordinates of the manipulator, the control torque of attitude $\boldsymbol{\tau}_{\mathbf{c}} \in R^{3\times 1}$ is relative to the center of mass coordinate. $\boldsymbol{\tau}_{\boldsymbol{\theta}} \in R^{n\times 1}$ is the joint of generalized control torque, $M_{11}(\mathbf{q}) \in R^{3\times 3}$, $M_{12}(\mathbf{q}) \in R^{3\times n}$, $M_{21}(\mathbf{q}) \in R^{n\times 3}$, $M_{22}(\mathbf{q}) \in R^{n\times n}$ are inertial matrix, $C_1(\mathbf{q},\dot{\mathbf{q}}) \in R^{3\times n}$, $C_2(\mathbf{q},\dot{\mathbf{q}}) \in R^{n\times n}$ are the n dimensional vector representing centrifugal and coriolis forces, $G(\mathbf{q}) \in R^{3\times 3}$ is the transform matrix.

In this paper, attitude control is the key to research so that there are no parameters relative to the orbit position of space robot.

3 Control System Design of Space Robot

In attitude control flying, space robot has some implies that existing:

1) Body's inertia is much greater than joint
2) Attitude, velocity of attitude, joint angle and speed of joint angle can be obtained.

Joint control torque can be obtained based on (2)

$$\boldsymbol{\tau}_{\boldsymbol{\theta}} = M_{22}(\mathbf{q})\mathbf{u} \tag{4}$$

So the acceleration of joint can be given by

$$\ddot{\boldsymbol{\theta}} = \mathbf{u} - \boldsymbol{\eta} \tag{5}$$

Where $\mathbf{u}$ is the control, the disturbance $\boldsymbol{\eta}$ is due to centrifugal and coriolis forces and it is given by

$$\boldsymbol{\eta} = M_{22}^{-1}\left(M_{21}\ddot{\boldsymbol{\varphi}} + C_2(\mathbf{q},\dot{\mathbf{q}})\dot{\mathbf{q}}\right) \tag{6}$$

Feedback control law is

$$\ddot{\boldsymbol{\theta}}^d - \ddot{\boldsymbol{\theta}} = -K_{p1}\left(\boldsymbol{\theta}^d - \boldsymbol{\theta}\right) - K_{d1}\left(\dot{\boldsymbol{\theta}}^d - \dot{\boldsymbol{\theta}}\right) - \left(\Delta\mathbf{u} - \boldsymbol{\eta}\right) \tag{7}$$

Where θ^d is the vector of desired joint angles, K_{p1} and K_{d1} are feedback gains, $\Delta\mathbf{u}$ is the compensate term of disturbance $\boldsymbol{\eta}$.

Based on equation (6), the closed-loop system can be written as

$$\dot{\mathbf{x}} = A\mathbf{x} + B\left(\boldsymbol{\eta} - \Delta\mathbf{u}\right) \tag{8}$$

Where

$$\mathbf{x} = \begin{bmatrix} \mathbf{x}_1 \\ \mathbf{x}_2 \end{bmatrix} = \begin{bmatrix} \boldsymbol{\theta}^d - \boldsymbol{\theta} \\ \dot{\boldsymbol{\theta}}^d - \dot{\boldsymbol{\theta}} \end{bmatrix} \tag{9}$$

$$A = \begin{bmatrix} 0 & I \\ -K_{p1} & -K_{d1} \end{bmatrix} \quad B = \begin{bmatrix} 0 \\ -I \end{bmatrix} \tag{10}$$

Several important properties of space robot may be derived

1) Generalized coordinates are bounded
2) With the fuel exhaust, inertia improved, and many other uncertainty prosperities as follows

$$\left\|M_{21}(\mathbf{q})\right\| \le \alpha_1 \tag{11}$$

$$\lambda_m \le \left\|M_{22}(\mathbf{q})\right\| \le \lambda_M \tag{12}$$

$$\|\boldsymbol{\eta}\| \le \boldsymbol{\rho} \tag{13}$$

α_1, λ_m and λ_M are the given positive parameters.

Define

$$\boldsymbol{\eta} = \sum_{j=1}^{3+n} \dot{q}_j D_{1j} \dot{\mathbf{q}} + D_2 \ddot{\boldsymbol{\varphi}} \tag{14}$$

Where

$$D_{1j} = M_{22}^{-1} C_{2j} \qquad D_2 = M_{22}^{-1} M_{21} \tag{15}$$

So the results can be obtained based on equation (14), (15)

$$\rho(t) = \eta^{\max}(i) = \sum_{j=1}^{3+n} \sum_{k=1}^{3+n} \left| d_{ijk} \right| \left| \dot{q}_j \dot{q}_k \right| + \sum_{k=1}^{3} \left| d_{ik} \right| \left| \ddot{\varphi}_k \right| \tag{16}$$

d_{ijk} and d_{ik} are respectively the k elements of the i column in D_{1j} and D_2.That $d_{ijk=} D_{1j}(i,k)$ $d_{ik=} D_2(i,k)$. Solution of $\eta^{\max}(i)$ can be referenced paper[10].

Lmma1 (Global exponential stability) taken into the system

$$\dot{\mathbf{x}} = \mathbf{f}(\mathbf{x}, t) \qquad \mathbf{x}(t_0) = \mathbf{x}_0 \tag{17}$$

Assumption that there exist $V(\mathbf{x}, t)$, λ_1 and λ_2, yields to

$$\lambda_1 \|\mathbf{x}\|^2 \le V(\mathbf{x}) \le \lambda_2 \|\mathbf{x}\|^2 \qquad \dot{V}(\mathbf{x}) \le -\lambda_2 \|\mathbf{x}\|^2 + \gamma \exp(-\beta t) \tag{18}$$

If $\lim_{t \to \infty} \gamma \exp(-\beta t) = 0$ then (17) is global exponential stability. Because state matrix A is positive definite, there is positive definite matrix $P > 0$, yields to

$$A^T P + PA = -Q \tag{19}$$

Where Q is positive definite matrix. The control law is designed to compensate the disturbance $\boldsymbol{\eta}$.

$$\Delta \mathbf{u} = -\frac{\rho(t) \cdot PB\mathbf{x}}{\|PB\mathbf{x}\| + \gamma \exp(-\beta t)} \tag{20}$$

Stability of the robust controller can be proved based on (21)

$$V(\mathbf{x}) = \frac{1}{2} \mathbf{x}^{\mathrm{T}} P \mathbf{x} \tag{21}$$

Then derivation (21)

$$\begin{aligned}\dot{V}(\mathbf{x}) &= \frac{1}{2}\dot{\mathbf{x}}^{\mathbf{T}} P\mathbf{x} + \frac{1}{2}\mathbf{x}^{\mathbf{T}} P\dot{\mathbf{x}} \\ &= -\frac{1}{2}\mathbf{x}^T Q\mathbf{x} + \mathbf{x}^{\mathbf{T}} PB(\Delta\mathbf{u} - \boldsymbol{\eta}) \\ &\le -\frac{1}{2}\mathbf{x}^T Q\mathbf{x} + \mathbf{x}^{\mathbf{T}} PB\Delta\mathbf{u} + \left\|\mathbf{x}^T PB\right\|\|\boldsymbol{\eta}\| \\ &\le -\frac{1}{2}\mathbf{x}^T Q\mathbf{x} + F_1 + F_2 \\ &\le -\frac{1}{2}\mathbf{x}^T Q\mathbf{x} + \frac{\left\|\mathbf{x}^T PB\right\|\rho(t)}{\|PB\mathbf{x}\| + \gamma\exp(-\beta t)}\gamma\exp(-\beta t) \\ &\le -\frac{1}{2}\mathbf{x}^T Q\mathbf{x} + \rho(t)\gamma\exp(-\beta t)\end{aligned} \tag{22}$$

Where

$$F_1 = \frac{-\mathbf{x}^{\mathbf{T}} PB(PB\mathbf{x})\rho(t) + \left\|\mathbf{x}^T PB\right\|\|PB\mathbf{x}\|\rho(t)}{\|PB\mathbf{x}\| + \gamma\exp(-\beta t)} \tag{23}$$

$$F_2 = \left\|\mathbf{x}^T PB\right\|\rho(t)\gamma\exp(-\beta t) \tag{24}$$

Therefore, the robust controller is taken as

$$\tau_u = M_{22}(\theta)\Delta\mathbf{u} \qquad \tau_L = M_{22}(\theta)(\mathbf{u} - \Delta\mathbf{u}) \tag{25}$$

$$\boldsymbol{\tau}_{\boldsymbol{\theta}} = \boldsymbol{\tau}_L + \boldsymbol{\tau}_u \tag{26}$$

4 Simulation and Analysis

In order to verify the effect of the designed robust controller, the corporative simulation of trajectory tracking and attitude control is accomplished. Space robot with 5 degree of freedom and its mathematical model can be obtained in equations (1) and (2).

Attitude controller is by PD controller and the control parameters

$$K_{p2} = [800 \quad 2900 \quad 2000] \quad K_{d2} = [460 \quad 1970 \quad 1270]$$

besides, mass of the system center is the inertial mass coordinates origin and the original parameters in inertial mass coordinates as follows

Initial Attitude (rad): $\varphi(0) = [0.0698 \quad 0.0349 \quad 0.0349]^T$

Desired trajectory of attitude: $\varphi^d = [0 \quad 0.0010663t \quad 0]^T$

Initial joint angels: $\theta = \mathbf{0}$

Table 1. Parameters of space robot

Parameters	Base	L1	L2	L3	units
Link length		0.6	1	1	m
mass	400	40	30	30	kg
Ixx	80	1	1	1.3	
Iyy	96	5	3	3	
Izz	40	0.8	2.8	0.5	(Kg*m2)
Ixy	35	-0.08	-0.28	0.01	
Ixz	-38	-0.8	4	3	
Iyz	-35	0.17	0.08	-0.3	

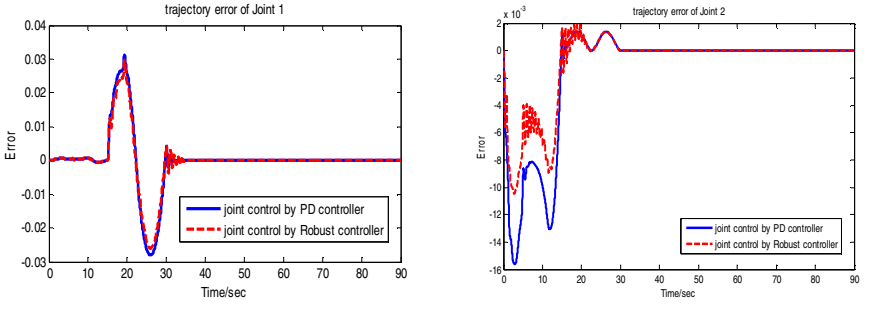

Fig. 1. Trajectory tracking error (end effecter no load)

Fig.1 shows the result of joint trajectory tracking. There is still minimal oscillation and tracking error when PD is the control strategy. However, space manipulator can be controlled in accordance with the desired position. In contrast, robust controller has better performance than PD controller.

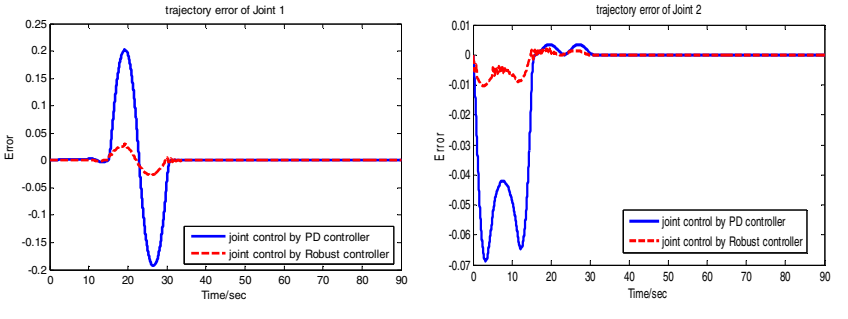

Fig. 2. Trajectory tracking error (end effecter with load)

Fig.2 shows the result of trajectory tracking error and the target is in end effecter. In task space, there is serious tracking error for vary of inertia when joint motion is controlled by PD controller. Conversely, robust controller has a better performance.

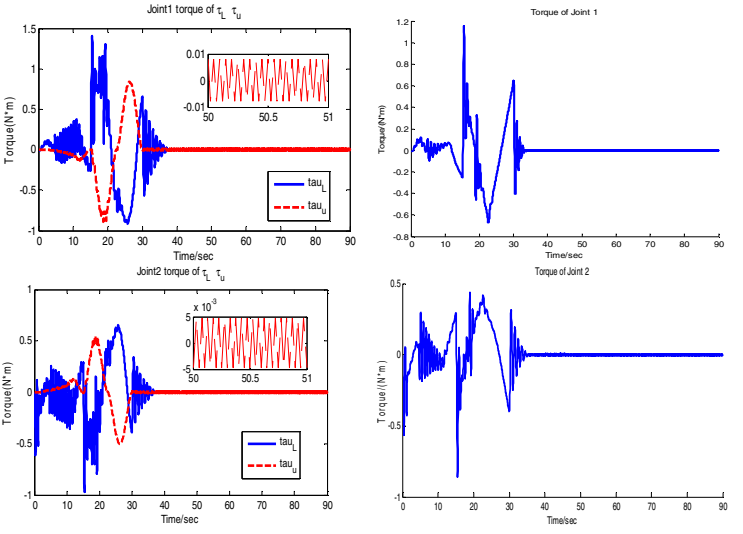

Fig. 3. Torque of Joint 1 and Joint 2 (end effecter no load)

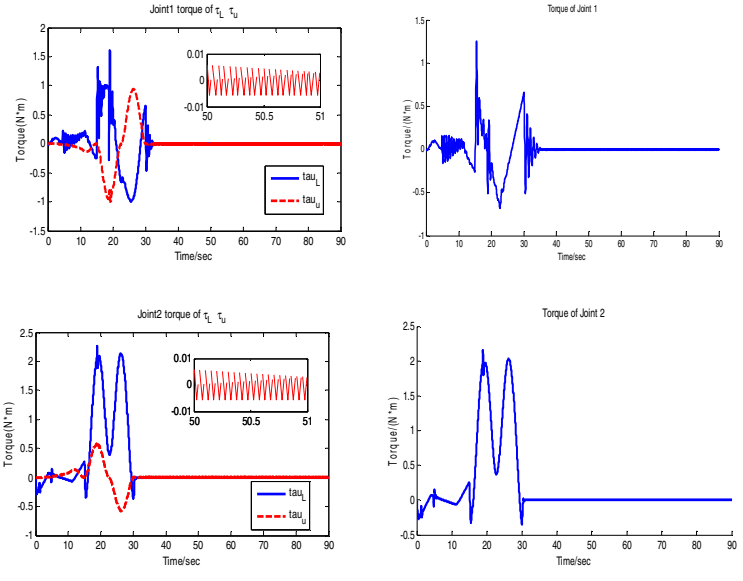

Fig. 4. Torque of Joint 1 and Joint 2 (end effecter with load)

From Fig.3-Fig.4, it is that the torque is different between end effecter no load and end effecter with load; τ_L and τ_u are a complementary relation so that the control torque can be decreased; The torque of Joint 2 is higher when space manipulator in docking mode.

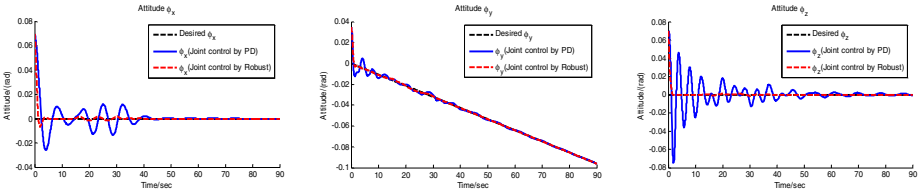

Fig. 5. Attitude trajectory tracking (end effecter with load)

Conclusion

In this paper, robust controller is improved. Trajectory tracking is much better than paper[11]; Torque of Joint can be analyzed and there are much more fuel will be saved. Besides, attitude control is more easily.

Acknowledgements. The authors would like to thank the editors and referees of this proceeding. This work is supported by East red Satellite Company.

References

1. Matsuda, K., Kanemitsui, Y.H., Kijimoto, S.: Attitude control of a space robot using the nonholonomic structure. In: AIAA (1998)
2. Feng, B., Ma, G., Wen, Q., Wang, C.: Design of Robust Intelligent Controller for Space Robot in Task Space. Journal of Astronautics (April 2007)
3. Gu, Y.L., Xu, Y.S.: A normal form augmentation approach to adaptive control of space robot systems. In: Conf. on Robotics and Automation, Atlanta, USA, pp. 731–737 (1993)
4. Chen, L.: Adaptive and robust composite control of coordinated motion of space robot system with prismatic joint. In: Intelligent Control and Automation, China (2002)
5. Xu, W.: Path Planning for Base Attitude Adjustment of a Free-floating Space Robot System. Robotics 28(3), 291–296 (2006)
6. Green, A., Sasiadek, J.Z.: Intelligent Tracking Control of a Free-Flying Flexible Space Robot Manipulator. In: Navigation and Control Conference, AIAA-2007-6320 (2007)
7. Yime, E., Saltaren, R., Diaz, J.: Robust adaptive control of the Stewart-Gough robot in the task space. In: American Control Conference (ACC), pp. 5248–5253 (2010)
8. Liu, M.: Decentralized PD and robust nonlinear control for robot manipulators. Journal of Intelligent and Robotic Systems 20(2), 319–332 (1997)
9. Seweryn, K., Banaszkiewicz, M.: Optimization of the Trajectory of a General Free – Flying Manipulator during the Rendezvous Maneuver. In: AIAA Guidance, Honolulu (2008)
10. Xu, G., Zhang, M.: Robust control of One Arm Space Manipulator. In: IPTC (2011)

Design of Quasi-periodic Satellite Formation at Critical Inclination

Guangyan Xu, Huanqiang Wang, and Meng Zhang

School of Automation, Shenyang Aerospace University
110136, Shenyang, China
Guangyan_xu@163.com

Abstract. Periodic or quasi-periodic satellite formations can minimize the active control of long-term satellite formation flying. In this paper, a design of quasi-periodic satellite formation is proposed. The quasi-periodic constrains and mean relative motion of the member satellite under J_2 perturbation are used. The reference orbit must be at the critical inclination with a small eccentricity. The quasi-periodic constrains can release more DOFS to design the geometry formation than strict J_2 invariant trajectory conditions. The osculating orbital elements are used in numerical simulation, the design is proved to be correct through the simulation.

Keywords: satellite formation; J_2 perturbation; quasi-periodic conditions; relative orbit; osculating orbital elements.

1 Introduction

With the development of the space technology, the small satellite formation technology has become an issue research. There are many important properties in the frozen orbit, so designing satellite formations on the orbit has important significance. It is very necessary to design the satellite formations, analyses the effect of all kinds of perturbations and research the formation maintenance and control at critical inclination.

Many scholars have already done a lot of work on satellite formation research. Chris Sabol, Hanspter and Schaub etc have got important achievements by using the Hill or improved Hill equation in [1][2]. The design has been researched by Zhang Yu-kun through the kinematics and dynamics and the perturbation is analyzed in [3], however, the small eccentricity elliptical orbit of reference satellite is not analyzed; Guoqiang Zeng has put forward a general design of the satellite formation and the effect of various perturbations is analyzed through numerical method in [4]. We do a lots work on the periodic or quasi-periodic satellite formation design and perturbation analysis at critical inclination and make some achievements in [5][6].

In this paper, a design of quasi-periodic satellite formation is proposed. The reference orbit must be at the critical inclination with a small eccentricity. The osculating orbital elements are used in numerical simulation, it show the satellite formation can accommodate J_2 perturbation effectively, so the design is proved to be correct.

D. Yang (Ed.): Informatics in Control, Automation and Robotics, Volume 2, LNEE 133, pp. 67–74.
springerlink.com

2 Design of Quasi-periodic Satellite Formation

A passive and periodic satellite formation is critical to sustain a long-term formation flying mission. It is proved in [7][8] that the passive and periodic satellite formations in classical Keplerian motion can be achieved as long as every satellite in the formation has the same orbital period *T*, which is equivalent to having the same mean motion $\dot{M}$, or same semi-major axis *a*.

$$\delta T = 0 \Leftrightarrow \delta \dot{M} = 0 \Leftrightarrow \delta a = 0 \tag{1}$$

A passive and periodic satellite formation accommodating the J_2 perturbation will ensure long-term flying formation practically possible. Including the J_2 gravity term into the classical Keplerian motion causes the secular growths of three mean orbit elements $(\bar{\Omega}, \bar{\omega}, \bar{\mathrm{M}})$ i.e., the right ascension of the ascending node $\bar{\Omega}$, the argument of perigee $\bar{\omega}$ and the mean anomaly $\bar{\mathrm{M}}$. The J_2 perturbation lead the rates of differential orbit elements in [6] as

$$\delta\dot{\bar{\Omega}} = \frac{3J_2R_e^2\sqrt{\mu}}{4\bar{a}^{9/2}\bar{\eta}^5}\left(7c_{\bar{i}}\bar{\eta}\delta\bar{a} + 2\bar{a}\left(4c_{\bar{i}}\delta\bar{\eta} + s_{\bar{i}}\bar{\eta}\delta\bar{i}\right)\right) \tag{2}$$

$$\delta\dot{\bar{\omega}} = -\frac{3J_2R_e^2\sqrt{\mu}}{8\bar{a}^{9/2}\bar{\eta}^5}\cdot 7\left(5c_{\bar{i}}^2 - 1\right)\bar{\eta}\delta\bar{a} - \frac{3J_2R_e^2\sqrt{\mu}}{8\bar{a}^{9/2}\bar{\eta}^5}\cdot 2\bar{a}\left(4\left(5c_{\bar{i}}^2 - 1\right)\delta\bar{\eta} + 5\bar{\eta}s_{2\bar{i}}\delta\bar{i}\right) \tag{3}$$

$$\delta\dot{\bar{M}} = \frac{3\sqrt{\mu}}{2\bar{a}^{5/2}}\left(\frac{7J_2R_e^2}{4\bar{a}^2\bar{\eta}^3}\left(1-3c_{\bar{i}}^2\right) - 1\right)\delta\bar{a} + \frac{9J_2R_e^2\sqrt{u}}{4\bar{a}^{7/2}\bar{\eta}^4}\left(\left(1-3c_{\bar{i}}^2\right)\delta\bar{\eta} - \bar{\eta}s_{2\bar{i}}\delta\bar{i}\right) \tag{4}$$

Where $s_{(\cdot)} = \sin(\cdot), s_{(\cdot)} = \cos(\cdot)$ .Over bars denotes the secular part of a variable. $\bar{\eta} = \sqrt{1-\bar{e}^2}$ is another expression of eccentricity *e*. *i* denotes orbit inclination. J_2 , R_e and$\mu$are J_2 coefficient, equatorial radius and gravitational constant of the Earth respectively.

Some researchers [9] suggested confining a formation by only one constraint, i.e., matching the nodal orbital period only

$$\delta T = 0 \Leftrightarrow \frac{\delta\dot{\bar{M}}}{\eta} + \delta\dot{\bar{\omega}} + \delta\dot{\bar{\Omega}}\cos\bar{i} = 0 \tag{5}$$

This condition is known as the no-drift condition. On one side, this condition can be taken as the general case of the period matching condition (1) of the unperturbed Keplerian motion. On another side, since both the strict J_2 invariant relative orbit conditions in [10] and the J_2 invariant relative orbit conditions in [11] ensure the no-drift condition (5), the no-drift condition can also be viewed as a general case of another two J_2 invariant relative orbit conditions.